Catalysis Today 151 (2010) 314–329

Contents lists available at ScienceDirect

Catalysis Today

journal homepage: www.elsevier.com/locate/cattod

Modeling the effect of Pt dispersion and temperature during anaerobic regeneration of a lean NO_x trap catalyst

Divesh Bhatia, Michael P. Harold *, Vemuri Balakotaiah **

Department of Chemical & Biomolecular Engineering, University of Houston, Houston, TX, United States

ARTICLE INFO

Article history:
Available online 15 April 2010

Keywords:
Diffusion
Crystallite
NO_x reduction
NO_x trap
LNT model
Ammonia
Spillover

ABSTRACT

A crystallite-scale model is incorporated into a reactor-scale model to study the effect of Pt dispersion and temperature during the regeneration of a lean NO_x trap (LNT) comprising a Pt/BaO catalyst. The current study is based on a recent experimental study [R.D. Clayton, M.P. Harold, V. Balakotaiah, C.Z. Wan, Appl. Catal. B 90 (2009) 662]. The model shows that an increase in the Pt dispersion for a fixed Pt loading increases the interfacial perimeter between Pt and Ba, and has a significant effect on the regeneration kinetics. The transient product distribution displayed by three catalysts having varied Pt dispersions (3.2%, 8% and 50%) is explained by the localized stored NO_x gradients in the Ba phase. A rate determining process during the regeneration is found to be the diffusion of stored NO_x within the Ba phase towards the Pt/Ba interface. Temperature-dependent NO_x diffusivities in the Ba phase are used to predict the breakthrough profiles of H_2, N_2 and NH_3 over a range of catalyst temperatures. Finite gradients in the stored NO_x concentration are predicted in the Ba phase, thus showing that the nitrate ions are not sufficiently mobile at lower temperatures for the low dispersion catalysts. The model predicts that the highest amount of NH_3 is produced by the low dispersion catalyst (3.2% dispersion) at high temperatures, by the high dispersion catalyst (50% dispersion) at low temperatures, and by the intermediate dispersion catalyst (8% dispersion) at intermediate temperatures, consistent with the experimental data. It is found that the net NH_3 generation is favored under conditions when NO_x transport to the Pt/Ba interface is the rate determining process. The model considers the consumption of chemisorbed oxygen on Pt by H_2, which is used to predict the low effluent N_2 concentration for the 50% dispersion catalyst as compared to the 8% dispersion catalyst. Finally, a novel design is proposed to maximize the amount of NH_3 in the effluent of a LNT, which can be used as a feed to a selective catalytic reduction (SCR) unit placed downstream of the LNT.

1. Introduction

Due to the increasingly stringent NO_x emission standards for automobiles, active research is underway to limit the NO_x emissions. Several NO_x reduction technologies under development in recent years have now been commercialized, including selective catalytic reduction (SCR) with NH_3 or hydrocarbons, and NO_x storage and reduction (NSR). The focus of the current work is NSR, which is carried out in a monolithic reactor containing a multifunctional catalyst. During the storage phase, NO_x is stored on the catalyst in the form of nitrites/nitrates, whereas the reduction phase involves regenerating the catalyst by reducing the stored NO_x with reductants, such as H_2, CO and hydrocarbons. The rational design, optimization, and control of the lean NO_x trap (LNT) requires a reactor model that captures the essential chemical and physical rate processes.

NSR models of varying complexity have been developed by a number of research groups in concert with experimental studies [2–25]. Surveys were provided by Guthenke et al. [26] and Roy and Baiker [27]. Some of the key studies relevant to the current study are highlighted here. Sharma et al. [3] developed a lean NO_x trap model in which Langmuir–Hinshelwood kinetics were used for the NO_x storage and reduction with propylene. This model was further upgraded by Sharma et al. [4], using a multi-step NO_x storage model developed earlier by Olsson et al. [6]. Tuttlies et al. [25] modeled the effect of the increase in the storage phase volume during NO_x uptake, resulting in pore diffusion limited NO_x storage. Olsson et al. [7] followed with a global model which used the shrinking core concept to describe the NO_x storage. A LNT model based on global kinetics for storage and reduction was developed in our group [2,28]. This model uses the concept of fast and slow storage sites,

* Corresponding author at: Department of Chemical and Biomolecular Engineering, University of Houston, 4800 Calhoun, S222 Engineering Building 1, Houston, TX 77204-4004, United States. Tel.: +1 713 743 4322.
** Corresponding author.
E-mail addresses: mharold@uh.edu (M.P. Harold), bala@uh.edu (V. Balakotaiah).

0920-5861/$ – see front matter © 2010 Elsevier B.V. All rights reserved.
doi:10.1016/j.cattod.2010.02.055

Nomenclature

a	width/hydraulic diameter of the channel (m)
A_{PF}	atomic packing factor
c_A	surface concentration of stored NO_x (mol/m^2 exposed BaO)
c_{Ao}	surface concentration of stored NO_x before start of regeneration (mol/m^2 exposed BaO)
c_A^*	dimensionless concentration of stored NO_x
c_j^{in}	inlet concentration of species j in the fluid phase (mol/m^3)
$c_j^{in^*}$	dimensionless inlet concentration of species j in the fluid phase
c_{jm}	cup-mixing concentration of species j in the fluid phase (mol/m^3)
c_{jm}^*	dimensionless cup-mixing concentration of species j in fluid phase
$c_{j,wc}$	concentration of species j at the fluid–washcoat interface (mol/m^3)
$c_{j,wc}^*$	dimensionless concentration of species j at fluid–washcoat interface
c_{Pt}	surface concentration of Pt (moles exposed Pt/m^2 exposed Pt)
C	constant to find instantaneous NO_x conversion (m^{-1})
C'	constant to find instantaneous NO_x conversion (s$^{-1/2}$)
d	Pt dispersion (%)
D_A	diffusivity of stored NO_x in the Ba phase (m^2/s)
D_{jm}	diffusivity of species j in the fluid phase (m^2/s)
D_{Pt}	diameter of a Pt atom (m)
F_j	effluent molar flow rate of species j (mol/s)
F_{NO}^o	inlet molar flow rate of NO during storage (mol/s)
I_P	perimeter of Pt/Ba interface per channel (m)
k_1	rate constant for NO_x regeneration by H_2 (m^4/mol s)
k_2	rate constant for NO_x regeneration by NH_3 (m^4/mol s)
k_3	rate constant for consumption of H_2 by chemisorbed oxygen (m^3/mol s)
$k_{c,j}$	mass transfer coefficient of species j (m/s)
K	proportionality constant for relating dispersion to crystallite radius (m)
L	length of the monolith (m)
m_{wc}	mass of washcoat (g)
M_{NO_x}	total moles of NO_x stored on the catalyst
M_{Pt_T}	total moles of Pt in the washcoat per channel
n_{ch}	total number of channels in the catalyst
N_{av}	Avogadro number
N_c	number of crystallites per channel
N_T	number of Pt atoms in the Pt crystallite
r	radial coordinate (m)
r^*	dimensionless radial coordinate
R_c	radius of the crystallite (m)
R_{eff}	radius over which NO_x is stored on exposed BaO (m)
R_Ω	effective transverse length scale (m)
S_{Baw}	total surface area of active BaO per unit mass of washcoat (m^2/g washcoat)
S_{BaO}	surface density of BaO (BaO molecules/m^2 exposed BaO surface)
S_E	exposed Pt surface area per channel (m^2)
t	time during the regeneration (s)
t_c	characteristic convection time (s)
t_{jD}	characteristic time for transverse diffusion of species j (s)
t_s	storage time (s)
t_{RA}	characteristic time for reaction of stored NO_x (s)
$t_{R_{H_2}}$	characteristic time for reaction of H_2 with stored NO_x (s)
$t_{R_{NH_3}}$	characteristic time for net generation of NH_3 (s)
t_{SD}	characteristic time for diffusion of stored NO_x in the Ba phase (s)
T_s	monolith temperature (K)
$\bar{u}$	average fluid velocity in the fluid phase (m/s)
x	axial coordinate (m)
$X^e_{NO_x stored}$	experimental instantaneous NO_x conversion (%)
$X^m_{NO_x stored}$	model-predicted instantaneous NO_x conversion (%)
z	dimensionless axial coordinate
δ_c	thickness of the washcoat (m)
ε_{wc}	porosity within the washcoat
τ	dimensionless time
λ	dimensionless radial distance
θ_v	fractional surface coverage of vacant sites on Pt
θ_{O-Pt}	fractional surface coverage of chemisorbed oxygen on Pt

corresponding respectively to the BaO sites in close proximity to the precious metal crystallites and others further removed [8,29,30]. The model predicts the experimentally observed spatio-temporal concentration profiles of reactants and products and the velocity of the H_2 concentration front during the regeneration under isothermal conditions. More complex NSR models in terms of the catalyst composition and the inlet gas composition have been proposed by various groups. The addition of CO_2 in the reactor feed was studied by Koci et al. [12] and Scholz et al. [21,22]. Koci et al. [10–12] used a large number of reactions in their global kinetic models, including the effect of ceria in addition to barium. The addition of ceria to a LNT catalyst was also incorporated in the kinetic models proposed by Konstantas and Stamatelos [18] and Koltsakis et al. [17].

A comprehensive understanding of the NO_x storage and reduction mechanism and kinetics ultimately requires a microkinetic description. Hence, microkinetic models which include the detailed surface chemistry on the catalyst have been proposed [5,23,24]. Xu et al. [5] described a microkinetic model for the steady-state NO reduction by H_2 in the presence of O_2. Larson et al. [23] also simulated the steady state NO_x reduction by H_2 and CO in the presence of O_2 using a microkinetic formulation. Finally, Lindholm et al. [24] developed a detailed microkinetic model for the NSR process in the presence of H_2O and CO_2.

Experimental studies by Pihl et al. [31], Cumaranatunge et al. [32], Mulla et al. [33], Clayton et al. [34] and Lietti et al. [35] showed that once formed, NH_3 serves as a hydrogen carrier which readily reacts with the stored NO_x. The reduction was found to be feed limited which led to the conclusion that the identity of the reductant or the reduction kinetics were unimportant [33]. Clayton et al. [34] later showed that kinetic limitations emerge at lower temperatures, resulting in reactivity differences between H_2 and NH_3. The spatio-temporal concentration profile during the regeneration predicted using a global model was shown by Bhatia et al. [2] to match the experimental trends at a moderate temperature (275 °C). However, the effect of temperature on the effluent profiles was not considered in the model. Recently, Clayton et al. [1] showed the effect of Pt dispersion on the formation of NH_3 using catalysts containing fixed amounts of Pt in the washcoat.

Using TPD and TPR measurements, Zhou et al. [36] concluded that the nitrate ions in the BaO phase are extremely mobile. However, isotopic experiments by Kumar et al. [37] using Temporal Analysis of Products (TAP) reactor showed that there are finite NO_x concentration gradients in the storage phase. Sakamoto et al. [38] used imaging techniques to show that NO_x was strongly adsorbed around an edge of Platinum. However, modeling studies to investigate the NO_x gradients in the Ba phase and their effects on the regeneration rate have not been reported in the literature.

The interaction between Pt and Ba in a LNT has been reported to be an important factor during the storage and reduction of NO_x by several research groups. Lindholm et al. [39] studied the effect of catalyst preparation on the storage and reduction performance of an LNT. They reported a higher NO_x storage capacity when Pt was added before Ba during the catalyst synthesis as compared to the reverse order of impregnation. The difference was especially evident at higher temperatures. This was explained by an increased contact between the Pt and Ba for the former case, which also resulted in an increased reduction efficiency. Elizundia et al. [40] carried out FT-IR studies and concluded that Pt-BaO interaction played a key role during NO_x storage on an LNT catalyst. Similar conclusions were drawn by other authors [29,30,41,42]. Spillover and reverse-spillover reactions have been considered in some of the modeling studies [6,24,25]. However, there are no detailed modeling studies in the literature which investigate the dependence of the Pt loading and dispersion on the interaction between Pt and Ba.

To our knowledge, all the NSR models that have appeared in the literature are valid for a specific catalyst. Hence, the kinetic constants need to be estimated separately for each catalyst using regression analysis of the experimental data. Moreover, studies aimed at modeling the effect of the catalyst loading have been mostly empirical in nature. For example, Scotti et al. [9] developed a kinetic model for NO_x storage based on the model proposed by Olsson et al. [6]. However, in order to account for the different catalysts used in the two studies, the Pt and Ba dispersions were used as adjustable parameters to predict the storage results.

The basis of the current modeling study is the experimental study reported by Clayton et al. [1], who examined the effect of Pt dispersion on the regeneration behavior of a $Pt/BaO/Al_2O_3$ catalyst under isothermal conditions. They analyzed the breakthrough profiles of H_2 and NH_3 for three catalysts having vastly different Pt dispersions (3–50%) at various temperatures. Certain data trends were explained by a rate limitation caused by the "reverse-spillover" of stored NO_x onto Pt. Also, they reported that the total amount of NH_3 produced during regeneration was a strong function of the Pt dispersion in addition to the catalyst temperature. The objective of the present study is to predict the observed effect of Pt dispersion on the amount of NH_3 formed and the breakthrough profiles of reactants and products at various temperatures. This is achieved by incorporating crystallite-scale details into a reactor-scale model. It is shown that the kinetics of NH_3 formation and consumption are fast and that a relatively simple description of the temperature-dependent diffusivity of NO_x within the Ba phase is able to predict the effluent concentration profiles. Finite NO_x concentration gradients within the Ba phase are predicted by the model, consistent with the TAP reactor studies recently reported by Kumar et al. [37].

2. Model development

First we summarize the experimental results, which were the basis for model development. $Pt/BaO/Al_2O_3$ catalysts having the same amount of Pt but varied dispersions (3.2%, 8% and 50%) were prepared, the details of which are mentioned elsewhere [1]. The weight percentage of Pt and BaO in the washcoat of these three catalysts was 2.48% and 13%, respectively. Storage experiments were carried out by feeding 500 ppm NO and 5% O_2 to the reactor; the amount of NO_x stored was fixed at ca. 1.5×10^{-5} moles for the three catalysts having different dispersions. This corresponds to ca. 1.15×10^{-4} moles stored NO_x/g washcoat, which was estimated from the reported washcoat mass fraction for the three catalysts. The storage was followed by a reduction of the catalyst with 1500 ppm H_2 (in inert Ar) for 200 s in the absence of O_2 to maintain isothermal conditions. The inlet gas flow rate for both the storage and regeneration was 1000 sccm. The effluent concentrations were measured and used to obtain the instantaneous NO_x conversion ($X^{e}_{NO_x stored}$), defined as

$$X^{e}_{NO_x stored} = \frac{\int_0^t [F_{NO_x}(t') + F_{NH_3}(t') + 2(F_{N_2O}(t') + F_{N_2}(t'))]\,dt'}{\int_0^{t_s} [F^{o}_{NO} - F_{NO_x}(t')]\,dt'} \quad (1)$$

Here F_j represents the effluent molar flow rate of species j, F^{o}_{NO} is the inlet molar flow rate of NO during the storage, and t_s represents the storage time. In these fixed NO_x storage experiments, the denominator was constant at 1.5×10^{-5} mol (within a reported 4% experimental error). It was observed that the regeneration of the 3.2% dispersion catalyst was slower as compared to the 8% and 50% dispersion catalysts. This was attributed by Clayton et al. [1] to a rate limitation involving the transport and reverse-spillover of stored NO_x onto Pt. The temperature was found to affect the regeneration rates as well. The difference in the reduction activity between the three catalysts was the highest at low temperatures ($<200\,^{\circ}C$). It was also observed that for the range of temperatures studied (160–370 °C), the largest amount of NH_3 was produced by the low dispersion catalyst (3.2% dispersion) at high temperatures, by the high dispersion catalyst (50% dispersion) at low temperatures, and by the intermediate dispersion catalyst (8% dispersion) at intermediate temperatures.

In the present work, the effect of Pt dispersion is explained by proposing a model which accounts for the varying amounts of Pt crystallites for the different catalysts and the resulting difference in the Pt/Ba interfacial perimeter. It is assumed that a stored NO_x species (represented by 'A' here) undergoes reverse-spillover via diffusion in the Ba phase towards the Pt/Ba interface, where it is reduced by H_2 as well as the reaction network intermediate, NH_3. The schematic in Fig. 1 shows a top view of the Pt crystallite (unshaded), whereas the outer shaded region represents the annular area over which NO_x is stored. Here, R_c is the radius of the crystallite and R_{eff} is the radius over which NO_x is stored on the

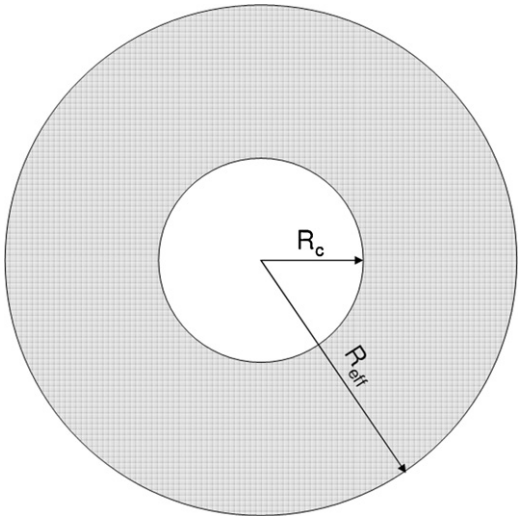

Fig. 1. Schematic of the top view of the Pt crystallite and the adjoining exposed BaO.

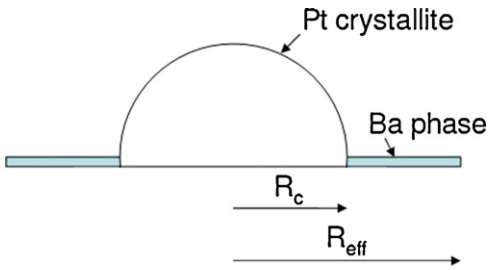

Fig. 2. Schematic of the exposed BaO and Pt crystallite.

barium phase. We will describe the method of estimating R_{eff} later. Fig. 2 is a side view of the Pt crystallite surrounded by the Ba phase. Assuming that the Pt crystallites have a hemispherical shape, the total number of Pt atoms in a crystallite (N_T) is obtained as

$$N_T = \frac{(2/3)\pi R_c^3 A_{PF}}{\pi D_{Pt}^3/6} \tag{2}$$

Here D_{Pt} is the diameter of a Pt atom and A_{PF} is the atomic packing factor. A value of 0.74 is used here for the A_{PF}, based on the FCC structure of Pt [43]. An average crystallite size is assumed since this is the extent to which the catalyst characterization was accomplished. The total number of crystallites per monolith channel, N_c, is obtained using the following relation:

$$N_c = \frac{M_{Pt_T} N_{av}}{N_T} \tag{3}$$

Here N_{av} represents the Avogadro number and M_{Pt_T} is the total number of moles of Pt in the washcoat (per channel). Using the expression for N_T from Eq. (2) in Eq. (3), we obtain the total number of crystallites per channel as

$$N_c = \frac{N_{av} D_{Pt}^3 M_{Pt_T}}{4 A_{PF} R_c^3} \tag{4}$$

The total exposed Pt area (S_E) and the total Pt/Ba interfacial perimeter (I_P) for a single channel are defined as

$$S_E = N_c 2\pi R_c^2 \tag{5}$$

$$I_P = N_c 2\pi R_c \tag{6}$$

Substituting the value of N_c from Eq. (4) into Eqs. (5) and (6), we get:

$$S_E = \frac{N_{av} D_{Pt}^3 \pi M_{Pt_T}}{2 A_{PF} R_c} \tag{7}$$

$$I_P = \frac{N_{av} D_{Pt}^3 \pi M_{Pt_T}}{2 A_{PF} R_c^2} \tag{8}$$

An increase in the Pt dispersion for a fixed Pt loading results in a reduction in the crystallite size [1]. Eqs. (7) and (8) expectedly show that for a fixed number of moles of Pt in the washcoat (M_{Pt_T}), an increase in the Pt dispersion, or equivalently a decrease in the particle size (R_c), results in an increase in the exposed Pt area (S_E) available for adsorption and the interfacial perimeter (I_P) available for NO_x reverse-spillover. It is also seen from Eq. (4) that the total number of crystallites increase with a decrease in the crystallite radius (or increase in dispersion), due to which the average distance between the Pt crystallites decreases.

In accordance with the isothermal regeneration modeling study done by our group [2], the following overall catalytic reactions are proposed to occur at the Pt/Ba interface:

1a. $8H_2 + Ba(NO_3)_2 \rightarrow 5H_2O + BaO + 2NH_3$
2a. $(10/3)NH_3 + Ba(NO_3)_2 \rightarrow 5H_2O + BaO + (8/3)N_2$

An additional reaction is proposed to occur on the exposed area of the Pt crystallites, and is given by

3a. $H_2 + O\text{–}Pt \rightarrow H_2O + Pt$

It should be noted that the stored NO_x is assumed to be present in the form of nitrates. However, at low temperatures, nitrites are likely to be present in the Ba phase in addition to nitrates. This is not considered in the present model, which would affect the quantitative accuracy of the model at low temperatures. However the trends of the effluent H_2 and NH_3 concentrations and NO_x conversions with respect to the temperature and Pt dispersion would be unaffected.

Assuming one-dimensional radial diffusion of stored NO_x within the Ba phase (refer to Fig. 1), the localized material balance for stored NO_x is given by

$$\frac{\partial c_A}{\partial t} = \frac{D_A}{r}\frac{\partial}{\partial r}\left(r\frac{\partial c_A}{\partial r}\right); \quad R_c \le r \le R_{eff} \tag{9}$$

with the initial and boundary conditions given by

$$\text{IC}: \quad \text{At } t = 0, \qquad c_A = c_{Ao}(r), \qquad R_c \le r \le R_{eff} \tag{10}$$

$$\text{BC1}: \quad \text{At } r = R_c, \qquad D_A\frac{\partial c_A}{\partial r} = k_1 c_A c_{H_2,wc} + k_2 c_A c_{NH_3,wc} \tag{11}$$

$$\text{BC2}: \quad \text{At } r = R_{eff}, \qquad \frac{\partial c_A}{\partial r} = 0 \tag{12}$$

Here c_A represents the concentration of the stored NO_x (in mol/exposed BaO area), D_A represents the diffusivity of stored NO_x in the Ba phase, r is the radial coordinate, and c_{Ao} is the concentration of stored NO_x before the start of regeneration. It is assumed that at the start of regeneration, NO_x is stored uniformly in the Ba phase in the radial direction. It is instructive to mention that if NO_x is stored only via the spillover mechanism, a gradient in the stored NO_x concentration in the Ba phase is likely to be present in the radial direction. However, the storage of NO_x can occur in the Ba phase even without the role of Pt. Hence, the concentration profile of stored NO_x in the Ba phase at the beginning of regeneration depends on the relative contribution of the spill-over mechanism and the adsorption/desorption of NO_x on/from the Ba phase. Thus, a storage model at the crystallite-scale is needed to accurately obtain the stored NO_x distribution in the Ba phase at the start of regeneration. In the absence of such a model in the literature, we assume a uniform distribution of stored NO_x in the Ba phase in the radial direction. Parameters k_1 and k_2 are the rate constants for the regeneration of stored NO_x by H_2 and NH_3, respectively, while $c_{H_2,wc}$ and $c_{NH_3,wc}$ are the concentrations of H_2 and NH_3 at the fluid–washcoat interface, respectively, at a particular axial point in the reactor. Eq. (11) assumes that the diffusional limitations in the washcoat (transverse to the flow) are negligible and that the diffusive flux of stored NO_x at the Pt/Ba interface is equal to its consumption by H_2 and NH_3. It was shown in an earlier study [2] that a LNT global kinetic model comprising of reactions (1a) and (2a) was able to predict the spatio-temporal evolution of reactants and products during anaerobic regeneration.

A simple calculation based on the weight fraction of BaO and the BET surface area of the catalyst showed that the amount of BaO in the catalysts used by Clayton et al. [1] is sufficient to cover the entire Al_2O_3 surface by a monolayer of BaO. This confirms earlier findings by Castoldi et al. [44] and Fanson et al. [45]. On the other hand, it has been shown by FT-IR studies that BaO might not cover all the Al_2O_3 sites [46]. Further evidence of exposed Al_2O_3 on the catalyst surface is the measured uptake of NO_2 at lower temperatures, which was reported by Clayton et al. [47]. It can be shown that even if we were to consider one-dimensional diffusion of NO_x from multiple BaO layers, the model predicted trends with respect to the catalyst dispersion and temperature would remain the same.

Table 1
Values of N_c, R_c and R_{eff} for various Pt dispersions.

Pt dispersion (%)	N_c	R_c (nm)	R_{eff} (nm)
3.2	7.18×10^{11}	15.0	195
8	9.93×10^{12}	6.25	52.7
50	1.82×10^{15}	1.1	4.02

Hence, for simplicity, we assume that BaO is present as a monolayer on the Al_2O_3 surface. As described before, R_{eff} is an estimate of the BaO that is utilized for NO_x storage. The value of R_{eff} can be obtained by equating the total moles of NO_x stored on the catalyst (M_{NO_x}) to twice the number of moles of exposed BaO, i.e.,

$$M_{NO_x} = \frac{2n_{ch}N_c S_{BaO}\pi(R_{eff}^2 - R_c^2)}{N_{av}} \quad (13)$$

Here, n_{ch} is the total number of channels in the catalyst, and S_{BaO} represents the surface density of BaO (BaO molecules/exposed BaO area over which NO_x is stored). Substituting N_c from Eq. (4) into Eq. (13), we get the expression:

$$R_{eff} = R_c\sqrt{1 + \frac{2A_{PF}M_{NO_x}R_c}{n_{ch}\pi S_{BaO}D_{Pt}^3 M_{Pt_T}}} \quad (14)$$

Expectedly, the size of the storage domain increases with the amount of NO_x stored. The ca. 1.5 order dependence of R_{eff} on R_c suggests that the storage domain size increases with an increase in R_c for a fixed Pt loading. In practical applications, the BaO sites would be occupied by species other than stored NO_x, such as H_2O, CO_2, etc. In the presence of these species, the value of R_{eff} would be higher than that given by Eq. (14), because of competitive adsorption of the various species on BaO. The values of N_c, R_c and R_{eff} for various values of the Pt dispersion are given in Table 1, and the parameters used to estimate these values are given in Table 2. The values of R_c and Pt dispersion have been measured and have been taken from Clayton et al. [1]. As they reported, the Pt particle size was not measurable for the 50% dispersion catalyst. Instead, the value of R_c was obtained using $2R_c(m) = (1.1 \times 10^{-9}/d(\%)) \times 100$, where d is the Pt dispersion [48]. The value of M_{NO_x} is taken from the fixed NO_x storage experiments; i.e. 1.5×10^{-5} mol NO_x were stored on all the three catalysts [1]. The value of M_{Pt_T} has been obtained using the Pt loading of the three catalysts (=95 g Pt/ft^3 catalyst or 204 mol Pt/m^3 washcoat). The value of S_{BaO} was obtained from the study by Bowker et al. [49] who reported that the BaO(1 1 1) surface, when prepared in a thin film form on Pt(1 1 1), presents a surface with twice the lattice parameter expected for that of the bulk termination, i.e. a (2×2) reconstruction. Even though the actual BaO surface on the catalyst might not be an ideal (1 1 1) surface, we use this value of S_{BaO} as a reasonable estimate. The total surface area of active BaO per unit mass of the washcoat (S_{Baw}) is given by the following expression:

$$S_{Baw} = \frac{n_{ch}N_c\pi(R_{eff}^2 - R_c^2)}{m_{wc}} \quad (15)$$

Table 2
Parameter values used to estimate N_c and R_{eff}.

Parameter	Numerical value
A_{PF}	0.74
D_{Pt}	2.78×10^{-10} m
M_{NO_x}	1.5×10^{-5} mol
M_{Pt_T}	5.55×10^{-7} mol/channel
n_{ch}	28
N_{av}	6.022×10^{23}
S_{BaO}	1.89×10^{18} BaO molecules/m^2 exposed BaO

Here m_{wc} represents the mass of the washcoat. Using Eqs. (13) and (15), we obtain the following expression which relates the active BaO surface area to the moles of NO_x stored:

$$S_{Baw} = \frac{M_{NO_x}N_{av}}{2m_{wc}S_{BaO}} \quad (16)$$

Using a value of 130 mg for m_{wc} and other parameter values from Table 2, the active surface area of BaO was found to be 18.4 m^2/g washcoat for all the three catalysts. This corresponds to 1.15×10^{-4} mol NO_x stored/g washcoat. The typical BET surface area reported for Pt/BaO/Al_2O_3 catalysts is ca. 100 m^2/g washcoat. Putting this value in Eq. (16), we get a NO_x storage capacity of 6.27×10^{-4} mol NO_x/g washcoat. This value corresponds to the maximum amount of NO_x that can be stored on the catalyst. Clayton et al. [47] reported a NO_x storage capacity of 4.5×10^{-4} mol NO_x/g washcoat. However, the maximum NO_x storage time was five minutes, due to which the moles of NO_x stored were less than the theoretical maximum value. Note that the theoretical maximum value is based on an assumed value of S_{BaO} [49]. A change in the surface structure and NO_x storage in the bulk storage phase could alter the theoretical maximum amount of NO_x that can be stored on the catalyst.

In addition to the equations for NO_x spillover, species balances are needed for the gas and solid phases for H_2, NH_3 and N_2. The species balance for component j in the fluid phase is given by

$$\frac{\partial c_{jm}}{\partial t} = -\bar{u}\frac{\partial c_{jm}}{\partial x} - \frac{k_{c,j}(x)}{R_\Omega}(c_{jm} - c_{j,wc}) \quad (17)$$

Here, j represents H_2, N_2 or NH_3, c_{jm} represents the cup-mixing concentration of species j in the fluid phase, and $c_{j,wc}$ represents the concentration of species j at the fluid–washcoat interface. The fluid velocity and the transverse diffusion length scale are represented by $\bar{u}$ and R_Ω, respectively. Position-dependent mass-transfer coefficients for each species j, represented by $k_{c,j}(x)$, are used to account for the transverse gradients. The position dependence obtained from Ramanathan et al. [50] is used here. For a channel of square cross-section and uniform washcoat thickness, the H_2 species balance in the solid phase is given by

$$\frac{\partial c_{H_2,wc}}{\partial t} = \frac{1}{\varepsilon_{wc}\delta_c(a + \delta_c)} \times \left[ak_{c,H_2}(x)(c_{H_2,m} - c_{H_2,wc}) - \frac{c_{H_2,wc}N_c 2\pi R_c}{4L}(4k_1\, c_A|_{r=R_c} + k_3 c_{Pt}\theta_{O-Pt}R_c)\right] \quad (18)$$

Here ε_{wc}, δ_c, L and a represent the porosity within the washcoat, thickness of the washcoat, length of the monolith and width of the channel, respectively. k_3 represents the rate constant for the reaction between H_2 and chemisorbed oxygen, given by $H_2 + O\text{–}Pt \rightarrow H_2O + Pt$. c_{Pt} represents the surface concentration of Pt (in moles of exposed Pt/exposed area of Pt), and θ_{O-Pt} is the fractional surface coverage of chemisorbed oxygen on Pt. Eq. (18) assumes that the reaction rate between H_2 and stored NO_x is proportional to the perimeter of the Pt/Ba interface, whereas the reaction between H_2 and chemisorbed oxygen is proportional to the surface area of exposed Pt atoms. Hence, the term '$4k_1\, c_A|_{r=R_c}$' in Eq. (18) represents the consumption of H_2 by stored NO_x, whereas the term '$k_3 c_{Pt}\theta_{O-Pt}R_c$' represents the consumption of H_2 by chemisorbed oxygen on the exposed Pt surface. A similar balance for NH_3 in the

solid phase is given by

$$\frac{\partial c_{NH_3,wc}}{\partial t} = \frac{1}{\varepsilon_{wc}\delta_c(a+\delta_c)} \times \left[a k_{c,NH_3}(x)(c_{NH_3,m} - c_{NH_3,wc}) + \frac{N_c 2\pi R_c\, c_A|_{r=R_c}(k_1 c_{H_2,wc} - (5/3)k_2 c_{NH_3,wc})}{4L} \right] \quad (19)$$

In deriving Eq. (19), we implicitly assume that NH_3 does not react with the chemisorbed oxygen on Pt. The term '$k_1 c_{H_2,wc}$' in Eq. (19) represents the generation of NH_3 (reaction 1a), whereas '$(5/3)k_2 c_{NH_3,wc}$' represents the consumption of NH_3 by stored NO_x (reaction (2a)). Reaction (2a) has also been used to develop the species balance equation for N_2 in the solid phase, given by

$$\frac{\partial c_{N_2,wc}}{\partial t} = \frac{1}{\varepsilon_{wc}\delta_c(a+\delta_c)} \times \left[a k_{c,N_2}(x)(c_{N_2,m} - c_{N_2,wc}) + \frac{N_c 2\pi R_c k_2\, c_A|_{r=R_c} c_{NH_3,wc}}{3L} \right] \quad (20)$$

A balance for the vacant sites on Pt has the following form:

$$\frac{\partial \theta_v}{\partial t} = k_3 c_{H_2,wc}\theta_{O-Pt} \quad (21)$$

Here θ_v represents the fractional surface coverage of vacant sites on Pt.

The initial and boundary conditions are given by Eqs. (22) and (23), respectively

$$\text{IC}: \quad \text{At } t = 0, \quad c_{jm} = 0, \quad c_{j,wc} = 0, \quad \theta_v = 0, \quad 0 < x \le L \quad (22)$$

$$\text{BC}: \quad \text{At } x = 0, \quad c_{jm} = c_j^{in} \quad (23)$$

c_j^{in} in Eq. (23) represents the inlet concentration of species j.

Eqs. (9)–(12) and (17)–(23) are non-dimensionalized using the following variables:

$$z = \frac{x}{L}, \quad r^* = \frac{r - R_c}{R_{eff} - R_c}, \quad \tau = \frac{tD_A}{(R_{eff} - R_c)^2}, \quad \lambda = \frac{R_c}{R_{eff} - R_c} \quad (24)$$

$$c^*_{jm} = \frac{c_{jm}}{c^{in}_{H_2}}, \quad c^*_{j,wc} = \frac{c_{j,wc}}{c^{in}_{H_2}}, \quad c^*_A = \frac{c_A}{c_{Ao}} \quad (25)$$

The non-dimensionalized equations are given by

$$\frac{\partial c^*_A}{\partial \tau} = \frac{\partial^2 c^*_A}{\partial r^{*2}} + \frac{1}{r^* + \lambda}\frac{\partial c^*_A}{\partial r^*} \quad (26)$$

$$\text{IC}: \quad \text{At } \tau = 0, \quad c^*_A = 1, \quad 0 \le r^* \le 1 \quad (27)$$

$$\text{BC1}: \quad \text{At } r^* = 0,$$

$$\frac{\partial c^*_A}{\partial r^*} = \frac{(R_{eff} - R_c)c^{in}_{H_2} c^*_A}{D_A}(k_1 c^*_{H_2,wc} + k_2 c^*_{NH_3,wc}) \quad (28)$$

$$\text{BC2}: \quad \text{At } r^* = 1, \quad \frac{\partial c^*_A}{\partial r^*} = 0 \quad (29)$$

$$\frac{\partial c^*_{jm}}{\partial \tau} = \frac{(R_{eff} - R_c)^2}{D_A}\left[-\frac{\bar{u}}{L}\frac{\partial c^*_{jm}}{\partial z} - \frac{k_{c,j}(z)}{R_\Omega}(c^*_{jm} - c^*_{j,wc}) \right] \quad (30)$$

$$\frac{\partial c^*_{H_2,wc}}{\partial \tau} = \frac{(R_{eff} - R_c)^2}{D_A \varepsilon_{wc}\delta_c(a+\delta_c)} \times \left[a k_{c,H_2}(z)(c^*_{H_2,m} - c^*_{H_2,wc}) - \frac{c^*_{H_2,wc} N_c 2\pi R_c}{4L}(4k_1 c_{Ao}\, c^*_A\big|_{r^*=0} + k_3 c_{Pt}\theta_{O-Pt} R_c) \right] \quad (31)$$

$$\frac{\partial c^*_{NH_3,wc}}{\partial \tau} = \frac{(R_{eff} - R_c)^2}{D_A \varepsilon_{wc}\delta_c(a+\delta_c)} \times \left[a k_{c,NH_3}(z)(c^*_{NH_3,m} - c^*_{NH_3,wc}) + \frac{c_{Ao} 2\pi R_c N_c\, c^*_A\big|_{r^*=0}(k_1 c^*_{H_2,wc} - (5/3)k_2 c^*_{NH_3,wc})}{4L} \right] \quad (32)$$

$$\frac{\partial c^*_{N_2,wc}}{\partial \tau} = \frac{(R_{eff} - R_c)^2}{D_A \varepsilon_{wc}\delta_c(a+\delta_c)} \times \left[a k_{c,N_2}(z)(c^*_{N_2,m} - c^*_{N_2,wc}) + \frac{N_c 2\pi R_c k_2\, c_{Ao} c^*_A\big|_{r^*=0} c^*_{NH_3,wc}}{3L} \right] \quad (33)$$

$$\frac{\partial \theta_v}{\partial \tau} = \frac{(R_{eff} - R_c)^2}{D_A} k_3 c^{in}_{H_2} c^*_{H_2,wc}\theta_{O-Pt} \quad (34)$$

$$\text{IC}: \quad \text{At } \tau = 0, \quad c^*_{jm} = 0, \quad c^*_{j,wc} = 0, \quad \theta_v = 0, \quad 0 < z \le 1 \quad (35)$$

$$\text{BC}: \quad At\ z = 0, \quad c^*_{jm} = c^{in^*}_j \quad (36)$$

$c^{in^*}_j$ in Eq. (36) represents the dimensionless inlet concentration of species j. It is observed from Eq. (26) that the curvature effect would be negligible if $\lambda \gg 1$ (or $R_{eff} \approx R_c$), i.e. NO_x is stored very close to the Pt/Ba interface. However, Eq. (26) reduces to the conventional cylindrical 2D equation for $\lambda \to 0$ (or $R_{eff} \gg R_c$).

3. Results and discussion

Before discussing the results, it is instructive to describe the expected transient profile of the instantaneous NO_x conversion for various catalysts and the reaction conditions. A linear relationship between the instantaneous NO_x conversion and time indicates the presence of H_2 feed rate limitations. This behavior is exhibited by the intermediate (8%) and high dispersion (50%) catalysts at high temperatures, the conditions under which the supply of NO_x by the process of diffusional transport and spill-over of NO_x is fast and hence is not the rate controlling process. If the transport of NO_x towards the Pt/Ba interface is the rate controlling process, it can be shown for $\lambda \to 0$ that the diffusive flux is proportional to $\sqrt{D_A/t}$, where t is the time during the regeneration. Hence, the integral NO_x conversion would be given by $C\sqrt{D_A t}$, where C is a constant depending on the catalyst and reaction conditions. Fig. 3 shows the experimentally measured instantaneous NO_x conversions for the 3.2% dispersion catalyst. Four different values of the constant,

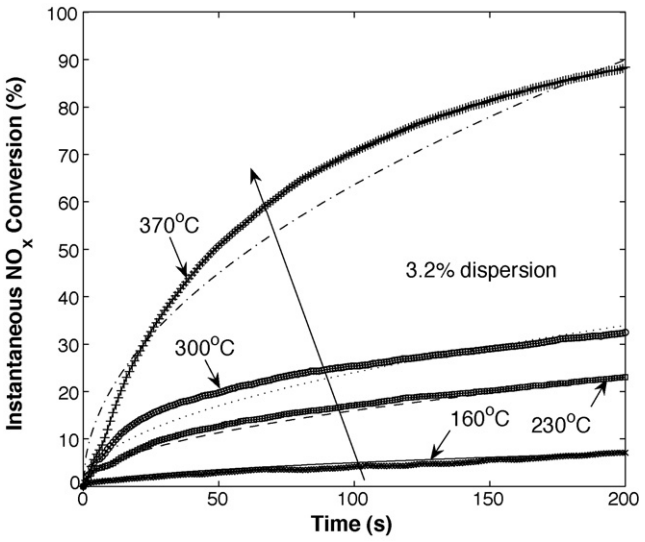

Fig. 3. Instantaneous NO_x conversion for various temperatures during regeneration of the 3.2% dispersion catalyst (markers represent experimental data; smooth lines represent predicted values).

C, are chosen and the instantaneous NO_x conversion ($X^{m}_{NO_x stored}$) is predicted using the relation: $X^{m}_{NO_x stored} = C'\sqrt{t}$, where $C' = C\sqrt{D_A}$. It is observed that the instantaneous NO_x conversion is proportional to the square root of time, hence indicating that the diffusion of stored NO_x is the rate determining process for the 3.2% dispersion catalyst. It is noted that the diffusional transport of stored NO_x and its spillover to the Pt are expected to be activated processes. Similar results were obtained for the 8% dispersion catalyst at low temperatures. This issue will be discussed in detail later.

An analysis of the characteristic times was performed in order to identify the rate determining process for a given operating condition. The following characteristic times were derived:

$$t_c = \frac{L}{\bar{u}}; \qquad t_{jD} = \frac{R_\Omega^2}{D_{jm}}; \qquad t_{SD} = \frac{(R_{eff} - R_c)^2}{D_A}; \qquad t_{RA} = \frac{R_{eff} - R_c}{k_1 c^{in}_{H_2}} \tag{37}$$

$$t_{R_{H_2}} = \frac{2\varepsilon_{wc}\delta_c(a+\delta_c)LA_{PF}R_c^2}{\pi k_1 c_{Ao} N_{av} D^3_{Pt} M_{Pt_T}};$$

$$t_{R_{NH_3}} = \frac{8\varepsilon_{wc}\delta_c(a+\delta_c)Lc^{in}_{H_2}A_{PF}R_c^2}{c_{Ao}\pi N_{av} D^3_{Pt} M_{Pt_T}(k_1 c_{H_2,wc} - \frac{5}{3}k_2 c_{NH_3,wc})} \tag{38}$$

The symbols, t_c, t_{jD}, t_{SD}, t_{RA}, $t_{R_{H_2}}$, and $t_{R_{NH_3}}$ represent the convection (or residence) time, diffusion time of species j in the transverse direction (synonymous with the external mass transfer time), characteristic diffusion time of stored NO_x in the Ba phase, characteristic reaction time for the consumption of stored NO_x, characteristic reaction time for the consumption of H_2 by NO_x, and characteristic reaction time for net generation of NH_3, respectively. The characteristic time for consumption of NO_x (t_{RA}) is derived using Eq. (28), whereas, $t_{R_{H_2}}$ and $t_{R_{NH_3}}$ are obtained using Eqs. (31) and (32), respectively, in combination with Eq. (4).

Table 3
Values of parameters used in the simulations.

Parameter	Numerical value
L	0.02 m
R_Ω	2.75×10^{-4} m
a	1.1×10^{-3} m
δ_c	3×10^{-5} m
ε_{wc}	0.4
k_1	1×10^{-3} m^4/(mol s)
k_2	1.5×10^{-5} m^4/(mol s)
k_3	10^5 m^3/(mol s)
c_{Ao}	6.28×10^{-6} mol/m^2 exposed BaO

Some of the physical and chemical properties used in the simulations and for the estimation of the characteristic times are given in Table 3. Temperature-dependent inlet gas velocities and the resulting inlet concentrations were used based on a total inlet flow rate of 1000 sccm in the experiments [1]. The gas-phase diffusivities (D_{jm}) of H_2, N_2, and NH_3 in Ar were obtained using the following relations, where T_s represents the monolith temperature:

$$D_{H_2,m} = 5.83 \times 10^{-9} T_s^{1.67} \tag{39}$$

$$D_{NH_3,m} = 1.62 \times 10^{-9} T_s^{1.70} \tag{40}$$

$$D_{N_2,m} = 1.213 \times 10^{-9} T_s^{1.70} \tag{41}$$

These relations were developed by calculating the gas-phase diffusivities of H_2, N_2 and NH_3 in Ar at different temperatures using Lennard–Jones potentials. The experiments used to model the effect of Pt dispersion and temperature were carried out for four different temperatures ranging between 160 and 370 °C [1]. For these temperatures, the values of inlet gas velocities, gas-phase diffusivities and the characteristic times, t_c, $t_{H_2,D}$, and $t_{NH_3,D}$ are given in Table 4. It is observed that the characteristic convection time decreases with temperature; this is a result of the increase in inlet gas velocities with temperature. Similarly, the characteristic transverse diffusion time for H_2 and NH_3 decreases with temperature due to an increase in the gas-phase diffusivity with temperature. It is observed that $t_{H_2,D} < t_c$ and $t_{NH_3,D} < t_c$, thus showing that transverse diffusion (or external mass transfer) is fast for both of the reacting gas phase species (H_2 and NH_3), and hence is likely not to limit the conversion of the gas phase species. Even though not shown here, the characteristic transverse diffusion time for N_2 was also found to be lower than the convection time for all the temperatures.

The values of the rate constants, i.e., k_1, k_2, and k_3 are required for the analysis of the characteristic reaction times. It was reported by Mulla et al. [33] that the identity of the reductant (H_2 or NH_3) and the associated reduction kinetics were unimportant during the regeneration at a high temperature (=300 °C). Also, it was shown earlier that the experimental NO_x conversion data indicated a rate limitation caused by the diffusion of NO_x towards the Pt/Ba interface (Fig. 3). Hence, the rate constants have been chosen such that a proportionate increase in each rate constant results in a negligible change in the predicted results, i.e. the rate of regeneration is not kinetically limited. Also, the kinetic constants are assumed to be independent of temperature. Note, however that this assumption is not valid at low temperatures since Clayton et al. [34] showed that kinetic differences between H_2 and NH_3 were observed at lower

Table 4
Estimated characteristic times at various temperatures.

T_s (°C)	$\bar{u}$ (m/s)	$D_{H_2,m}$ (m^2/s)	$D_{NH_3,m}$ (m^2/s)	t_c (s)	$t_{H_2,D}$ (s)	$t_{NH_3,D}$ (s)
160	7.77×10^{-1}	1.5×10^{-4}	5.0×10^{-5}	2.6×10^{-2}	5.1×10^{-4}	1.5×10^{-3}
230	9.03×10^{-1}	1.9×10^{-4}	6.5×10^{-5}	2.2×10^{-2}	3.9×10^{-4}	1.2×10^{-3}
300	1.03×10^{0}	2.4×10^{-4}	8.1×10^{-5}	1.9×10^{-2}	3.2×10^{-4}	9.4×10^{-4}
370	1.15×10^{0}	2.9×10^{-4}	9.8×10^{-5}	1.7×10^{-2}	2.6×10^{-4}	7.7×10^{-4}

Table 5
Estimated characteristic reaction times of stored NO_x (t_{RA}) for various dispersion catalysts at different temperatures.

	3.2%	8%	50%
160 °C	4.3×10^{-3} s	1.1×10^{-3} s	6.9×10^{-5} s
230 °C	5.0×10^{-3} s	1.3×10^{-3} s	8.1×10^{-5} s
300 °C	5.7×10^{-3} s	1.5×10^{-3} s	9.2×10^{-5} s
370 °C	6.4×10^{-3} s	1.6×10^{-3} s	1.0×10^{-4} s

temperatures. Clayton et al. [34] carried out NO reduction experiments using an equimolar mixture of H_2 and NH_3. For temperatures exceeding 150 °C, complete NO reduction by H_2 was observed with negligible conversion of NH_3, thus showing that NH_3 is not an effective reductant in the presence of H_2. Hence, the numerical value of k_2 is chosen to be much lower than k_1. Except for a sensitivity study, the selected values were not modified in any of the calculations carried out in this study.

An analysis of t_{RA} requires an estimate of the diffusivity of stored NO_x in the Ba phase, which to our knowledge is not available in the literature. We assume that the stored NO_x diffusivity at the four different temperatures, namely, 160, 230, 300 and 370 °C is 5×10^{-19}, 5×10^{-18}, 5×10^{-17}, and 5×10^{-16} m^2/s, respectively. These values correspond to a diffusion activation energy of ca. 75 kJ/mol, assuming an exponential dependence with temperature. We chose these values of diffusivity so that at the lowest diffusivity, the characteristic NO_x diffusion time (t_{SD}) is higher than the total time available for regeneration (200 s), whereas for the highest diffusivity, the characteristic stored NO_x diffusion time is less than the total time available for regeneration. This choice results in the prediction of incomplete NO_x conversions at low temperatures (corresponding to a low value of stored NO_x diffusion coefficient), and high conversions at high temperatures (or fast stored NO_x diffusion). We will return to this point later in the simulations.

The characteristic reaction times (t_{RA}) and diffusion times (t_{SD}) of stored NO_x for the three catalysts at different temperatures are given in Tables 5 and 6, respectively. The slight increase in the characteristic reaction times with an increase in temperature is due to the decreasing inlet concentration with temperature. The characteristic reaction time expectedly decreases with an increase in the Pt dispersion. It is observed that t_{SD} is higher than t_{RA} for each of the catalysts over the entire range of temperatures. Moreover, t_{SD} is higher than all the other characteristic times (t_c, t_{jD}, $t_{R_{H_2}}$), indicating that the diffusion of stored NO_x is the rate-determining process. This result was anticipated earlier using the dependence of the instantaneous NO_x conversion on the square root of time (Fig. 3). The analysis is valid when the regeneration is not limited by the inlet flow rate of the reductant. It is interesting to note that the diffusion of stored NO_x in a LNT catalyst is fundamentally similar to the diffusion of oxygen in a three-way catalytic converter (TWC) catalyst, which has been studied in more detail. For a ceria-supported TWC catalyst, Bedrane et al. [51] reported that oxygen storage on ceria is governed by the diffusion of oxygen, and that the storage is restricted to the ceria surface. This is similar to our finding that the stored NO_x diffusion is the rate-determining process. Using Eqs. (14) and (37), it can be shown that t_{SD} is proportional to the radius of the crystallite (R_c). Also, an increase in the dispersion would result in a decrease in the crystallite radius (Table 1). Hence, an increase in the dispersion would result in a reduction of the characteristic NO_x diffusion time, thus reducing the transport limitations. This trend can be seen in Table 6 and helps to explain the regeneration characteristics of the different dispersion catalysts. Also, since t_{SD} is inversely proportional to the diffusivity of stored NO_x in the Ba phase (Eq. (37)), the effect of temperature on the effluent concentrations can be explained by an increase in the diffusivity of stored NO_x with temperature. We will return to these points as well later in the paper.

Table 6
Estimated characteristic diffusion times of stored NO_x (t_{SD}) for various dispersion catalysts at different temperatures.

	3.2%	8%	50%
160 °C	6.5×10^4 s	4.3×10^3 s	1.7×10^1 s
230 °C	6.5×10^3 s	4.3×10^2 s	1.7×10^0 s
300 °C	6.5×10^2 s	4.3×10^1 s	1.7×10^{-1} s
370 °C	6.5×10^1 s	4.3×10^0 s	1.7×10^{-2} s

Eqs. (26)–(36) were solved for the set of parameters given in Tables 3 and 4 for three different Pt dispersions and various values of stored NO_x diffusivity. The value of c_{Pt} is obtained using $c_{Pt} = (M_{Pt_T}/N_c 2\pi R_c^2)(d/100)$; this gives 1.75×10^{-5}, 1.82×10^{-5}, and 2.0×10^{-5} mol/m^2 exposed Pt for the 3.2%, 8% and 50% dispersion catalysts, respectively. Position-dependent mass-transfer coefficients were used for a channel of square cross-section to incorporate the developing velocity and concentration fields in the front of the monolith [50]. Solid state and surface diffusivities as well as the diffusion activation energies vary markedly with the diffusing species as well as the substrate. For example, a diffusion activation energy of 60.6 kJ/mol has been reported for CO on Pt [52], resulting in a surface diffusivity of 2.73×10^{-18} m^2/s at 300 K. This is in contrast to an activation energy of 20.9 kJ/mol reported for CO on Ni(1 0 0) [53], which results in a surface diffusivity of 4.55×10^{-9} m^2/s at 300 K. In addition, the surface diffusivities of O at 300 K have been reported to be 9.04×10^{-22} m^2/s on W(2 1 1) [54], and as low as 1.47×10^{-25} m^2/s on W(1 1 0) [55]. These surface diffusivities correspond to an activation energy of 41.8–58.5 and 100 kJ/mol, respectively. Hence, surface and solid state diffusivities can vary by orders of magnitude from one system to the other. In the present work, the stored NO_x diffusivity was varied between 5×10^{-19} and 5×10^{-16} m^2/s to assess the model sensitivity to this parameter. As mentioned earlier, since the diffusivity of stored NO_x in the Ba phase is not available in the literature, we used the estimated characteristic times for stored NO_x diffusion to get estimates of the diffusivities. However, we stress that an attempt has not been made to fit the model-predictions to the experimental results.

Fig. 4(a) shows the experimentally measured temperature dependence of H_2 effluent concentrations when the low dispersion (3.2%) catalyst was exposed to 1500 ppm H_2 after storing 1.5×10^{-5} mol of NO_x. It is observed that at low temperatures, the effluent H_2 concentration increased sharply to its inlet value of 1500 ppm. However, for the highest temperature (370 °C), the H_2 effluent concentration increased slowly to its inlet value. These results can be explained by the rate limitations caused by the diffusion of stored NO_x towards the Pt/Ba interface. For the 3.2% dispersion catalyst, the average distance (R_{eff}) between the Pt/Ba interface and NO_x storage sites is quite large (195 nm; Table 1), rendering most of the NO_x stored inaccessible for regeneration by H_2. However, there is some NO_x stored close to the interface which gets regenerated at a rapid rate, even at low temperatures. The net result is a short period of no H_2 in the effluent, followed by a sharp H_2 breakthrough curve at low temperatures. As the temperature increases, the NO_x diffusivity increases, resulting in the faster transport of NO_x to the interface, where it reacts with H_2, resulting in a slow H_2 breakthrough. Fig. 4(b) shows the model-predicted effluent H_2 concentration for the 3.2% dispersion catalyst for various values of stored NO_x diffusivity. It is observed that the model is effectively able to capture the sharp H_2 breakthrough for low NO_x diffusivity (synonymous with low temperature), and a slow breakthrough at the highest value of diffusivity. The slight delay in the effluent H_2 concentration data as compared to the model-predicted results could be because of axial dispersion in the lines connecting

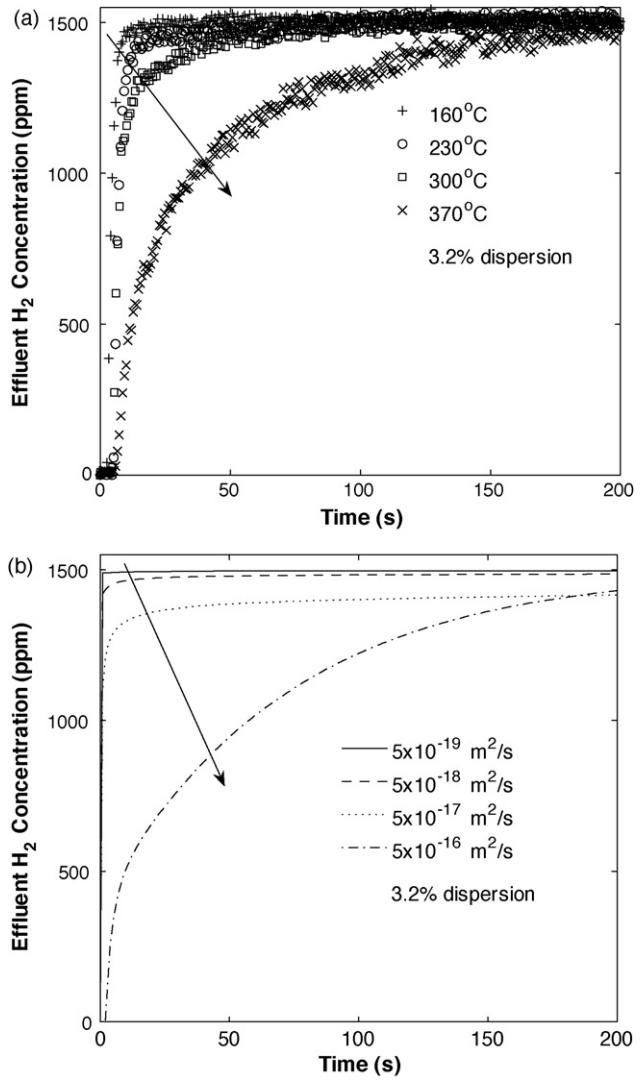

Fig. 4. (a) Experimental effluent H_2 concentrations at various temperatures for the 3.2% dispersion catalyst and (b) model-predicted effluent H_2 concentration for various stored NO_x diffusivities for the 3.2% dispersion catalyst.

the monolith reactor to the FT-IR apparatus. Such an effect is not captured in the model.

The corresponding temperature dependence of the model-predicted instantaneous NO_x conversions ($X^{m}_{NO_x stored}$) on time for various stored NO_x diffusivities is shown in Fig. 5, and is calculated as follows:

$$X^{m}_{NO_x stored}(t) = \frac{\int_0^t (F_{NH_3}(t') + 2F_{N_2}(t'))\,dt'}{M_{NO_x}} \quad (42)$$

Here F_{NH_3} and F_{N_2} represent the effluent molar flow rates of NH_3 and N_2, respectively. Note that the present model does not consider the formation of N_2O or NO_x release during regeneration. Hence, N_2O and NO_x have not been included in the model-predicted instantaneous NO_x conversion given by Eq. (42), as opposed to the experimental instantaneous NO_x conversion given by Eq. (1). Nevertheless, the results are similar to the experimentally measured NO_x conversion for various temperatures, shown in Fig. 3. At low temperatures (160 °C), the instantaneous NO_x conversion is low, whereas at high temperatures (370 °C), the NO_x conversion slowly increases, consistent with the slow breakthrough of H_2 (Fig. 4(a)). This is because the characteristic diffusion time (t_{SD}) given by Eq. (37) is inversely proportional to the diffusivity of NO_x in the BaO

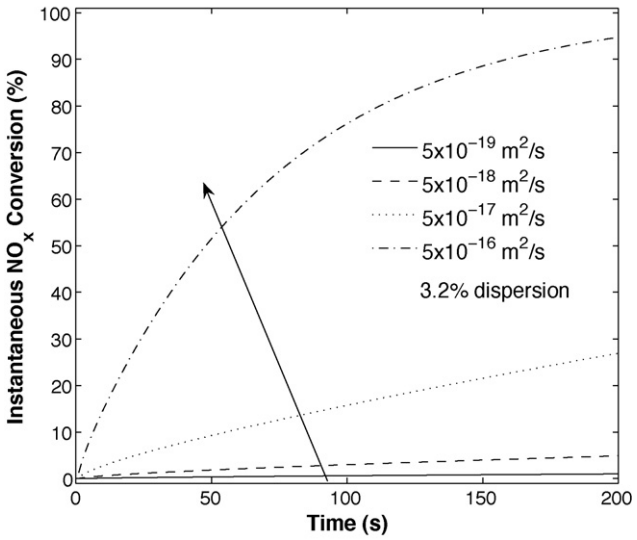

Fig. 5. Model-predicted instantaneous NO_x conversion for various stored NO_x diffusivities for the 3.2% dispersion catalyst.

phase. For low temperatures, the NO_x diffusivity is low resulting in a high characteristic time for diffusion, which leads to earlier breakthrough of H_2 and a low instantaneous NO_x conversion. With an increase in temperature, the NO_x diffusivity increases, reducing the characteristic diffusion times and thereby increasing the instantaneous NO_x conversions.

The effluent H_2 concentration profiles for the 8% dispersion catalyst at various temperatures are shown in Fig. 6(a). The H_2 breakthrough profiles for the 3.2% and 8% dispersion catalysts are compared using Figs. 4(a) and 6(a). It is observed that for a given temperature, the amount of H_2 consumed and hence the NO_x reduced during the regeneration is higher for the 8% dispersion catalyst as compared to the 3.2% dispersion catalyst. This is also observed by comparing the instantaneous NO_x conversions for the 3.2% and 8% dispersion catalysts, shown in Figs. 3 and 6(b), respectively. These trends can be explained by the dependence of the characteristic NO_x diffusion time (t_{SD}) on the catalyst dispersion. As described earlier, it can be shown using Eq. (14) that the characteristic diffusion time (t_{SD}) is proportional to the radius of the crystallite (R_c). Also, an increase in the Pt dispersion results in a decrease in the crystallite radius (Table 1). Hence, an increase of the Pt dispersion results in a reduction of the characteristic NO_x diffusion time, due to which the 8% dispersion catalyst would reduce more NO_x as compared to the 3.2% dispersion catalyst. This can also be explained in terms of the total exposed area of the Pt crystallites and the total interfacial perimeter available for NO_x reverse-spillover, given by Eqs. (7) and (8), respectively. The interfacial perimeter and the exposed Pt area are given in Table 7 for the varied dispersion catalysts. It is observed that increasing the Pt dispersion results in an increase in the interfacial perimeter in addition to the exposed Pt area. Thus, increasing the catalyst dispersion should result in increased rates for NO_x reverse-spillover and H_2 consumption by chemisorbed oxygen on the exposed Pt, due to increased Pt/Ba interfacial perimeter and exposed Pt area,

Table 7
Total interfacial perimeter and exposed Pt area for the varied dispersion catalysts. Refer to Eqs. (8) and (7).

d (%)	l_P (m/channel)	S_E (m^2/channel)
3.2	6.77×10^4	1.02×10^{-3}
8	3.90×10^5	2.44×10^{-3}
50	1.26×10^7	1.38×10^{-2}

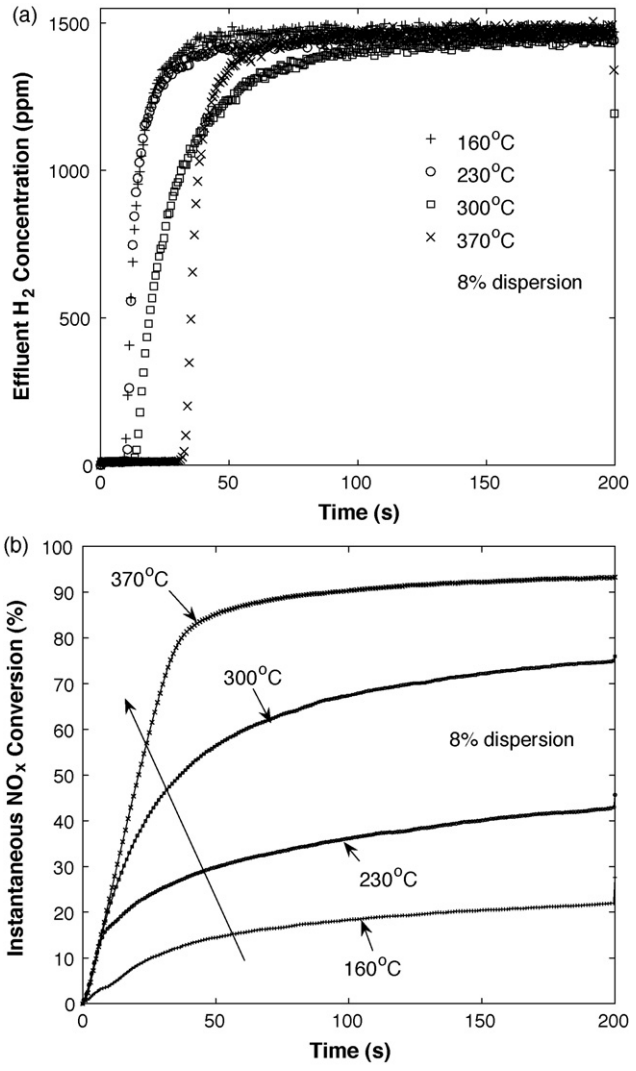

Fig. 6. (a) Experimental effluent H_2 concentration at various temperatures for the 8% dispersion catalyst and (b) experimental instantaneous NO_x conversion at various temperatures for the 8% dispersion catalyst.

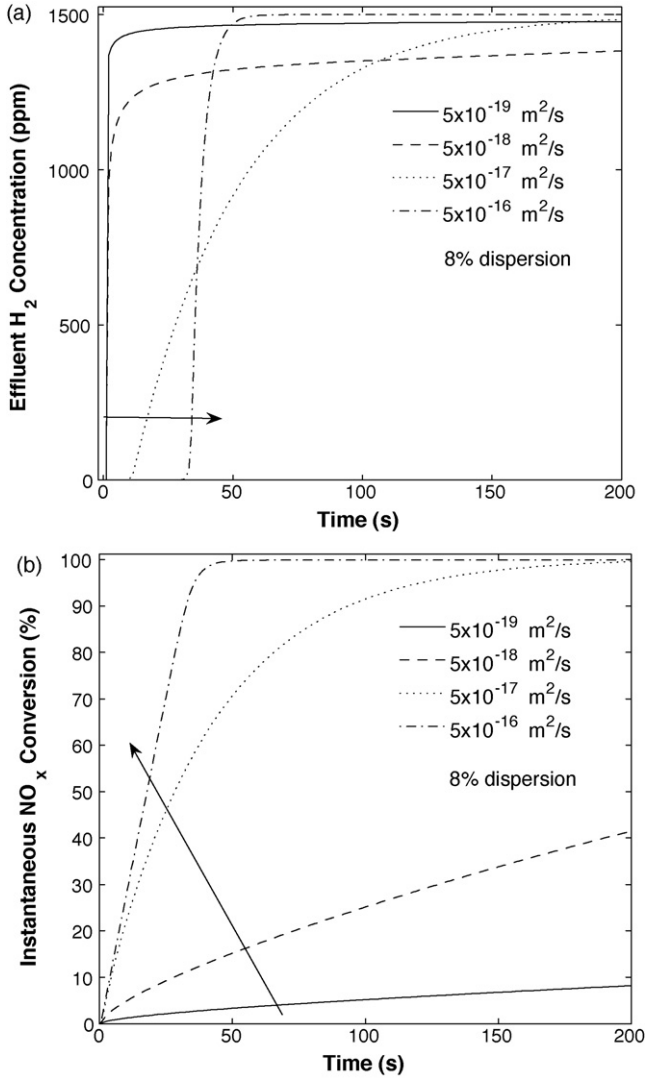

Fig. 7. (a) Model-predicted effluent H_2 concentration for various stored NO_x diffusivities for the 8% dispersion catalyst and (b) model-predicted instantaneous NO_x conversion for various stored NO_x diffusivities for the 8% dispersion catalyst.

respectively. The same concept can be used to explain the high NO_x conversions for the 50% dispersion catalyst as compared to the 3.2% and 8% dispersion catalysts.

From Fig. 6(a), it is observed that a sharp H_2 breakthrough occurs at low temperatures for the 8% dispersion catalyst similar to the 3.2% dispersion catalyst. An increase in temperature to 300 °C causes the slope of the H_2 breakthrough curve to decrease as was observed for the 3.2% dispersion catalyst at 370 °C. We attribute these observations to the increased rate of NO_x transport towards the Pt/Ba interface as was discussed for the 3.2% dispersion catalyst. On increasing the temperature further to 370 °C, a sharp H_2 breakthrough curve is again observed. A higher H_2 breakthrough time is a notable difference at this high temperature. Unlike at low temperatures, the sharp H_2 breakthrough at 370 °C is ascribed to the emergence of limitations caused by an inadequate H_2 supply feed rate as compared to the rate at which NO_x is regenerated. These experimental observations can be explained by assuming temperature-dependent diffusivities of stored NO_x. Fig. 7(a) shows the predicted effluent H_2 concentration for the 8% dispersion catalyst for various values of NO_x diffusivity. It is observed that the slope of the model-predicted H_2 breakthrough curve decreases and then increases with an increase in diffusivity, which is consistent with the experimental observations.

The change in the rate determining process resulting in a change in the slope of the H_2 breakthrough curves is more effectively depicted by analyzing the instantaneous NO_x conversions. Fig. 7(b) shows the model-predicted instantaneous NO_x conversion for the 8% dispersion catalyst for various stored NO_x diffusivities. For low values of diffusivity, the slope of the instantaneous NO_x conversion vs. time is low, conditions for which the overall process is diffusion controlled. However, as the diffusivity increases, the slope increases and for the highest diffusivity, a linear relationship is observed between the instantaneous NO_x conversion and time, indicating the aforementioned emergence of H_2 feed rate limitations. These results are similar to the experimentally measured instantaneous NO_x conversions at various temperatures for the 8% dispersion catalyst, shown in Fig. 6(b). It is noteworthy that the experimentally measured instantaneous NO_x conversions are less than 100%, even for the highest temperature (370 °C). This could be due to the experimental error in the calculation of stored NO_x during the storage phase. Another more likely cause is that some NO_x might be inaccessible to the reductant(s). Similar analysis was performed for the 50% dispersion catalyst. A linear relationship was observed between the instantaneous NO_x conversion and time for high temperatures (230, 300 and 370 °C), thus indicating that H_2

feed rate is the rate limiting process for the high dispersion (50%) catalyst.

As described earlier, the effluent concentration profiles are dependent on the reverse-spillover of NO_x towards the Pt/Ba interface, which in turn depends on the Pt dispersion and the temperature. Hence, the effect of temperature and Pt dispersion can be explained by analyzing the radial distribution of the stored NO_x concentration in the Ba phase ($R_c \le r \le R_{eff}$). The concentration of stored NO_x in the Ba phase at the end of the monolith ($x = L$) is shown in Fig. 8(a) for the 3.2% dispersion catalyst at the highest value of the stored NO_x diffusivity ($= 5 \times 10^{-16}\,m^2/s$), for various times during the regeneration. The concentration of stored NO_x prior to the regeneration is $6.28 \times 10^{-6}\,mol/m^2$ exposed BaO and was given in Table 3. It is observed that for all times during the regeneration, the NO_x concentration increases with distance from the Pt/Ba interface ($r = R_c$). The use of no-flux boundary condition (Eq. (12)) ensures a zero gradient of NO_x concentration in the radial direction at $r = R_{eff}$. As time progresses, more NO_x is transported towards the Pt/Ba interface due to its reduction by H_2 and/or NH_3. Hence, as seen in Fig. 8(a), the NO_x concentration decreases with time for a given radial position in the Ba phase. A radial gradient in the stored NO_x concentration at the exit of the reactor at $t = 10\,s$ suggests that the H_2 concentration front reaches the end of the monolith in less than 10 s, as was shown in Fig. 4(b).

The radial distribution of stored NO_x at the end of the monolith for a lower diffusivity ($5 \times 10^{-17}\,m^2/s$) is shown in Fig. 8(b) for the 3.2% dispersion catalyst. It is observed that in contrast to Fig. 8(a), the stored NO_x concentration is close to its initial value at all times near $r = R_{eff}$. This is attributed to the lower diffusivity of stored NO_x which results in lower NO_x conversions (Fig. 3). An analysis of the NO_x concentration was also performed for the 8% and 50% dispersion catalysts. The radial distribution of stored NO_x at the end of the reactor for the 8% dispersion catalyst at a diffusivity of $5 \times 10^{-16}\,m^2/s$ is shown in Fig. 8(c). It is observed that at shorter times (10 and 20 s), the stored NO_x concentration is equal to its initial value for all radial positions ($R_c \le r \le R_{eff}$). This is because the H_2 concentration front takes a finite time to reach the end of the reactor (Fig. 6(a)). It is also observed that because of the lower characteristic diffusion times for the 8% dispersion catalyst, the stored NO_x concentration reaches a value close to zero throughout the Ba phase towards the end of regeneration. Similar results were predicted for the 50% dispersion catalyst, except that the gradients within the Ba phase were small as compared to the 8% dispersion catalyst.

The computed concentration of the stored NO_x at the Pt/Ba interface ($r = R_c$) gives information about the rate determining process. A process limited by the diffusion of stored NO_x would result in low stored NO_x concentrations at the Pt/Ba interface as compared to the concentrations at $r = R_{eff}$. The interfacial NO_x concentration for the 3.2% dispersion catalyst for the range of diffusivities (5×10^{-19} to $5 \times 10^{-16}\,m^2/s$) was found to be close to zero, whereas the concentrations at $r = R_{eff}$ were much greater. This lends support to the diffusion of stored NO_x being the rate determining process. The interfacial NO_x concentrations were close to zero for the 8% dispersion catalyst as well for low diffusivities (5×10^{-19} and $5 \times 10^{-18}\,m^2/s$), suggesting again that the diffusion of stored NO_x is the rate determining process. However, as the diffusivity is increased further, the ratio of the interfacial concentration and the concentration at $r = R_{eff}$ increases to non-negligible values. This indicates the emergence of limitations caused by the feed rate of H_2 (Fig. 6(a)). Under these conditions, the radial profiles are characteristically more uniform since the stored NO_x diffusion is faster relative to the reductant feed rate.

The interfacial NO_x concentration for the 8% dispersion catalyst at the highest diffusivity ($5 \times 10^{-16}\,m^2/s$) is shown in Fig. 9(a).

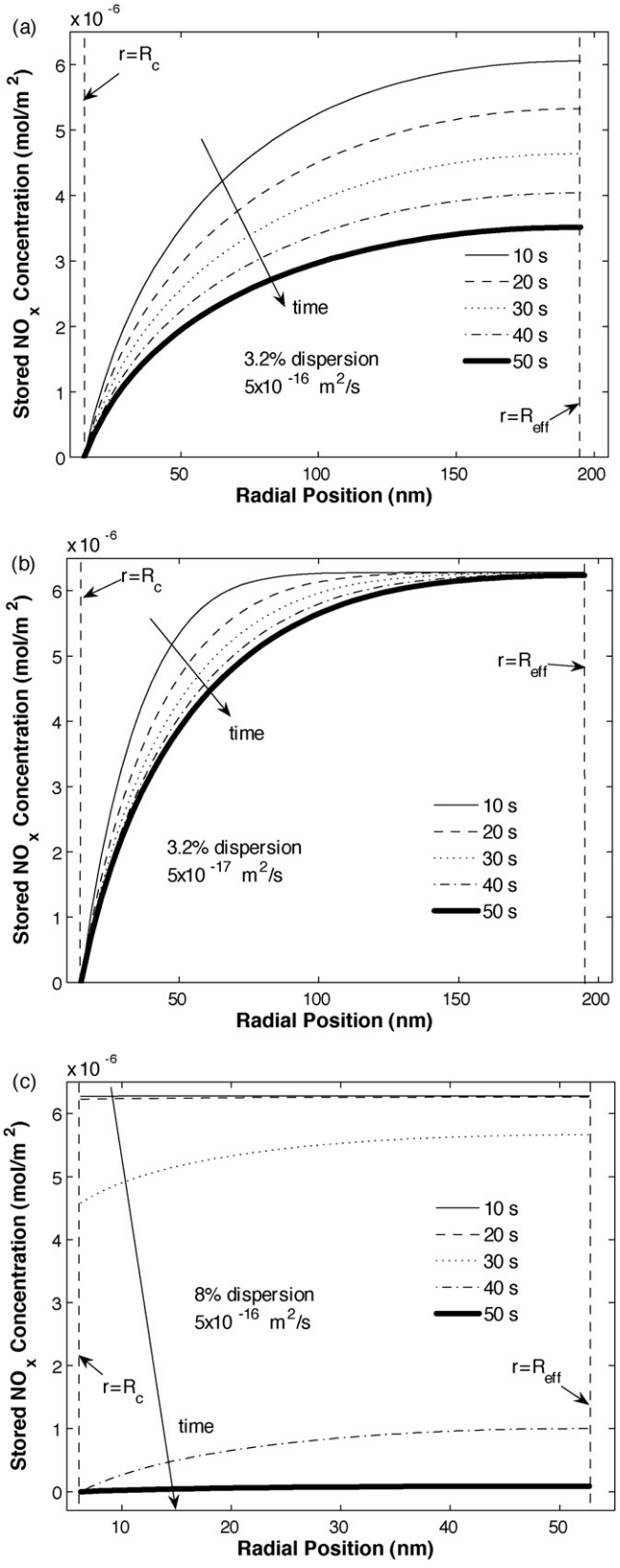

Fig. 8. Radial variation of the stored NO_x concentration at the monolith outlet for various times during the regeneration. (a) Dispersion = 3.2%, NO_x diffusivity = $5 \times 10^{-16}\,m^2/s$, (b) dispersion = 3.2%, NO_x diffusivity=$5 \times 10^{-17}\,m^2/s$ and (c) dispersion = 8%, NO_x diffusivity=$5 \times 10^{-16}\,m^2/s$.

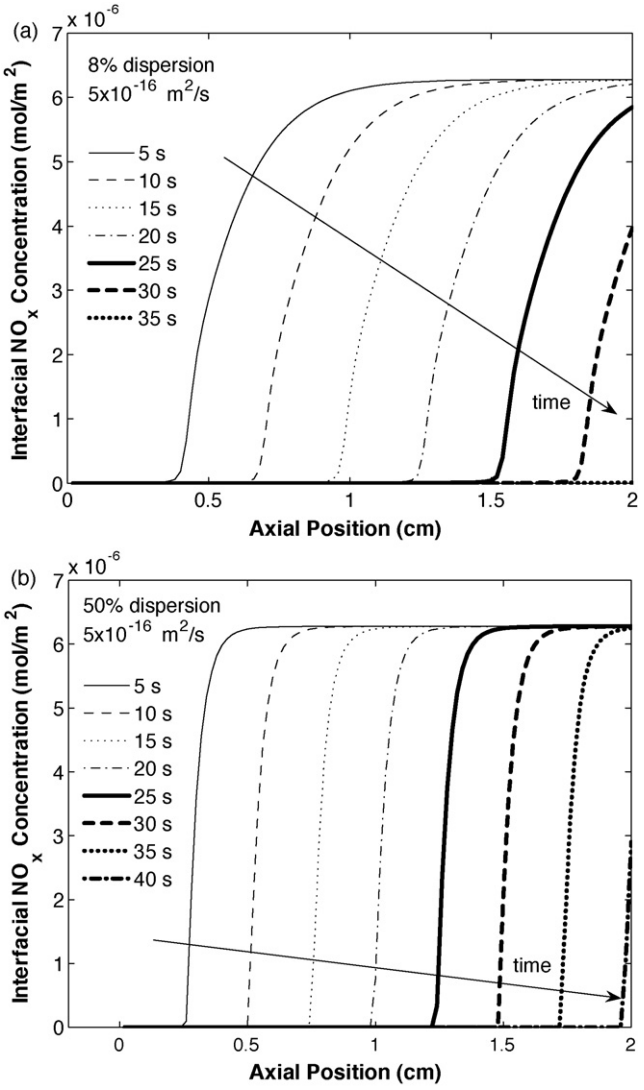

Fig. 9. Interfacial NO_x concentration for various times during the regeneration. (a) Dispersion = 8%, NO_x diffusivity=5×10^{-16} m^2/s and (b) dispersion = 50%, NO_x diffusivity=5×10^{-16} m^2/s.

It is observed that for all times, the interfacial NO_x concentration increases from zero to its highest value ($= c_{Ao}$). This can be related to the propagation of H_2 front along the length of the reactor. A zero interfacial NO_x concentration at the front of the reactor is due to its consumption by H_2. To the contrary, the interfacial NO_x concentration is equal to its initial value near the end of the reactor because the H_2 front does not propagate to the end of the reactor for low regeneration times. A non-zero interfacial concentration for the 8% dispersion catalyst at high diffusivity values supports our hypothesis that at high temperatures, the regeneration is limited by the feed rate of H_2. Similar analysis was performed for the 50% dispersion catalyst. The interfacial NO_x concentration for the 50% dispersion catalyst at the highest diffusivity (5×10^{-16} m^2/s) is shown in Fig. 9(b). A non-zero interfacial NO_x concentration was found for all the NO_x diffusivities, except in the front section of the reactor, suggesting that the regeneration is limited by H_2 feed rate. Similar to the 8% dispersion catalyst, the interfacial NO_x concentration increases from zero to its initial value along the length of the reactor. However, the concentration increase along the length is sharper as compared to the 8% dispersion catalyst. This can be explained by the higher reaction rates on the 50% dispersion catalyst.

Until now, the focus has been on the NO_x conversion and H_2 breakthrough curves. An important performance feature is the net production of NH_3 as evident in the NH_3 breakthrough curves. The measured effluent NH_3 concentrations for the 3.2%, 8% and 50% dispersion catalysts at various temperatures are shown in Figs. 10(a), (b) and (c), respectively. It is observed that for the 3.2% dispersion catalyst, the total amount of NH_3 produced increases with the temperature. For the 8% dispersion catalyst, the total NH_3 in the effluent exhibits a maximum with temperature, whereas it decreases monotonically with temperature for the 50% dispersion catalyst. These interesting trends can be explained by the current model, as discussed next.

It was shown earlier that the characteristic stored NO_x diffusion time (t_{SD}) is higher than all the other characteristic times, indicating that diffusion of stored NO_x towards the Pt/Ba interface may be the rate determining process during the regeneration. Calculation of the characteristic times using Eqs. (37) and (38) shows that $t_{R_{H_2}} < t_{RA}$, which indicates that the formation of NH_3 is governed by the characteristic reaction time for the consumption of stored NO_x (t_{RA}). Since stored NO_x is consumed by H_2 and NH_3, the selectivity to NH_3 is determined by the characteristic time for net NH_3 generation ($t_{R_{NH_3}}$). The ratio of $t_{R_{H_2}}$ and $t_{R_{NH_3}}$ is obtained from Eq. (38) and is given as

$$\frac{t_{R_{H_2}}}{t_{R_{NH_3}}} = \frac{1}{4c_{H_2}^{in}}\left(c_{H_2,wc} - \frac{5k_2c_{NH_3,wc}}{3k_1}\right) \tag{43}$$

As expected, Eq. (43) indicates that the selectivity to NH_3 is determined by the ratio of the rate constants, k_1 and k_2. Simulations were performed in which the rate constants, k_1 and k_2, were increased by the same factor for all the three catalysts ($k_3 = 0$ in these simulations). These modifications led to only a negligible change in the predicted H_2 and NH_3 effluent concentrations for each catalyst, hence validating our analysis of the characteristic reaction times.

The model-predicted effluent NH_3 concentration for the 3.2% dispersion catalyst for various stored NO_x diffusivities is shown in Fig. 11(a). It is observed that the model predicts an increase in the total effluent NH_3 with an increase in the diffusivity of stored NO_x (or temperature), which is consistent with the experimental results (Fig. 10(a)). As described earlier for the 3.2% dispersion catalyst, the rate limiting process during the regeneration is the transport of NO_x towards the Pt/Ba interface at all temperatures, due to which the interfacial NO_x concentration approaches zero. With an increase in the temperature, the rate of NO_x transport to the Pt/Ba interface increases, resulting in an increase in the NH_3 formation. Since NH_3 is not an effective reductant in the presence of H_2, H_2 reacts preferentially with the stored NO_x and most of the NH_3 formed appears in the effluent. This explains the increase in NH_3 formation with an increase in the temperature. Finally, it is observed from Figs. 10(a) and 11(a) that there is a slight delay in the experimental NH_3 effluent concentration as compared to the model-predicted results. This delay is not due to the subsequent reaction of NH_3 to form N_2, since negligible N_2 was observed in the effluent at low temperatures (not shown here). The likely cause for the delay in NH_3 is its adsorption on the catalyst. In a related modeling study, it was shown that the experimentally measured NH_3 and H_2O profiles during regeneration could be predicted by considering their adsorption on the catalyst surface [2]. However, for simplicity, the adsorption effects are not considered in the present model. The presence of axial dispersion in the lines connecting the reactor to the FT-IR apparatus could also contribute to the observed delay in NH_3. Negligible N_2 in the effluent at low temperatures shows that NH_3 is not an effective reductant under conditions where the diffusion of stored NO_x is the rate determining process. The inefficacy of NH_3 as a reductant under NO_x diffusion controlled regime is because under such conditions, H_2 is present at the Pt/BaO interface in addition to NH_3.

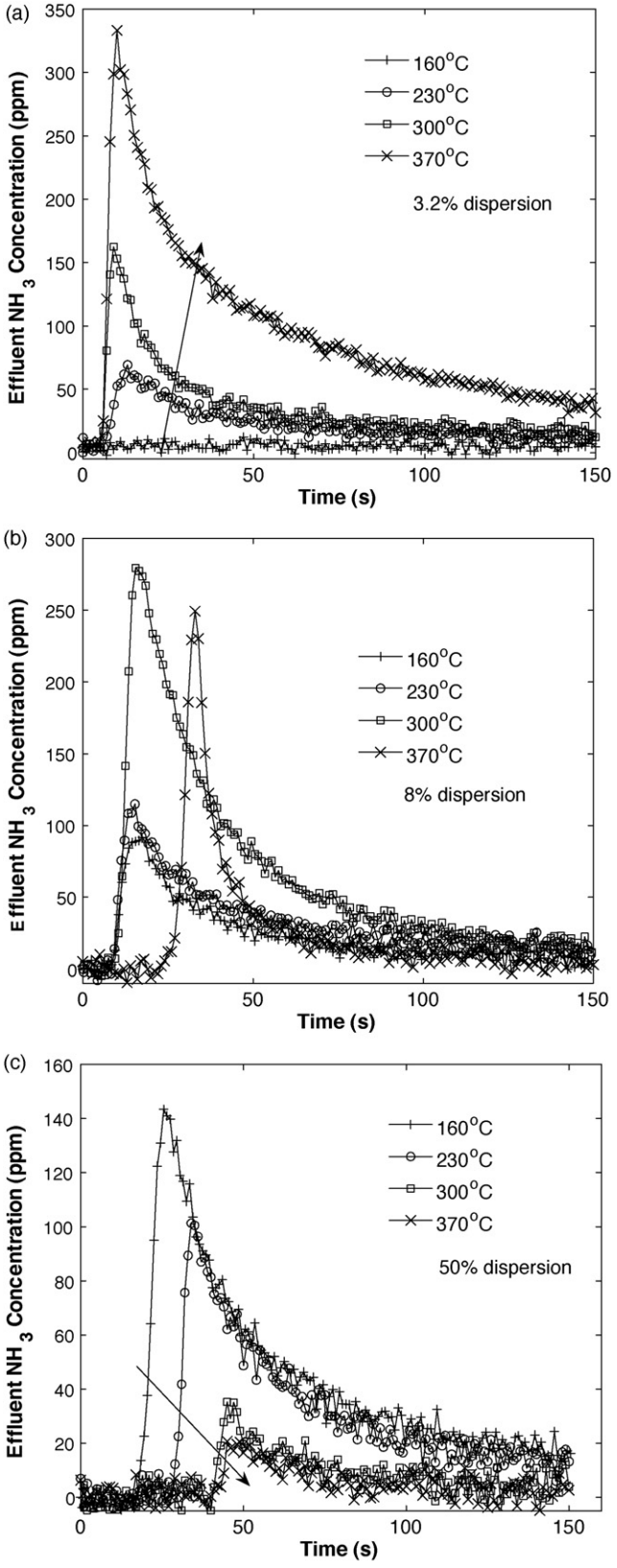

Fig. 10. Experimental effluent NH_3 concentration at various catalyst temperatures for the (a) 3.2% dispersion catalyst, (b) 8% dispersion catalyst and (c) 50% dispersion catalyst.

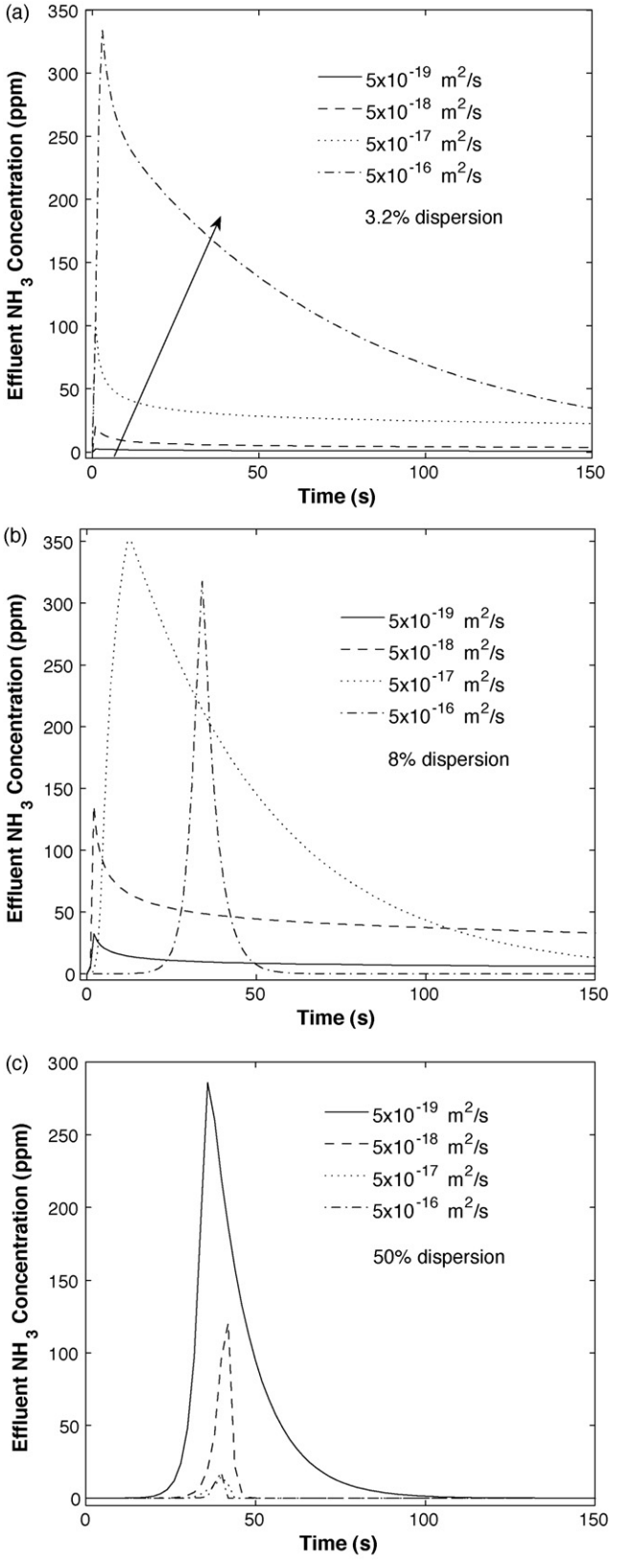

Fig. 11. Model-predicted effluent NH_3 concentration for various stored NO_x diffusivities for the (a) 3.2% dispersion catalyst, (b) 8% dispersion catalyst and (c) 50% dispersion catalyst.

Even though not shown here, the model predicts low values of effluent N_2 concentration at low temperatures for the 3.2% dispersion catalyst.

The model-predicted effluent NH_3 concentration for the 8% dispersion catalyst is shown in Fig. 11(b). It is observed that the model predicts a maximum in the peak NH_3 concentration with an increase in the diffusivity of stored NO_x. The results are similar to the experimentally observed maximum in the peak NH_3 concentration with respect to the catalyst temperature, shown in Fig. 10(b). As for the 3.2% dispersion catalyst, the NH_3 concentration increases with an increase in the diffusivity of stored NO_x. Under these conditions, the regeneration is governed by the transport of stored NO_x to the interface. However, with further increase in the stored NO_x diffusivity to 5×10^{-16} m^2/s, there is a shift in the rate limiting process from NO_x transport-limited to H_2 feed rate limited, which was discussed before in relation to Figs. 7(a) and (b). This results in non-zero interfacial NO_x concentrations. Under H_2 feed rate limited conditions, all the H_2 reacts to form NH_3, conditions for which NH_3 does not compete with H_2 for the stored NO_x. Hence, the stored NO_x at the interface reacts with NH_3, which results in a decrease of effluent NH_3 concentration for the highest stored NO_x diffusivity. Figs. 10(b) and 11(b) reveal that the model-predicted peak NH_3 concentration is higher than the experimentally measured values. A plausible reason for this could be NH_3 adsorption on the catalyst, which has not been considered in the present model.

The model-predicted effluent NH_3 concentration for various stored NO_x diffusivities for the 50% dispersion catalyst is shown in Fig. 11(c). The model predicts a decrease in total NH_3 in the effluent with an increase in the diffusivity of stored NO_x. The decrease in the amount of NH_3 with temperature was observed experimentally (Fig. 10(c)). For the 50% dispersion catalyst, feed rate limitations are observed at all the temperatures (except 160 °C). As discussed earlier, NH_3 does not compete with H_2 for the stored NO_x under H_2 feed rate limited conditions. With an increase in the temperature, the rate of NO_x transport to the Pt/Ba interface increases, resulting in a higher concentration of stored NO_x at the interface. This increases the NH_3 consumption rates, thereby decreasing the effluent NH_3 concentration. However, the predicted effluent NH_3 concentration is higher than the experimentally measured concentrations at all the temperatures. As stated before, this is likely a cause of NH_3 adsorption on the catalyst, which is strongly favored at low temperatures. Another factor could be the accuracy of the value of R_c used in the simulations for the 50% dispersion catalyst. As mentioned before, the Pt particles were not measurable for the 50% dispersion catalyst, due to which the radius of the crystallite was estimated using the value of Pt dispersion.

To summarize, NH_3 formation is favored under conditions when NO_x transport to the Pt/Ba interface is the rate determining process. This is more likely for the low dispersion catalysts, as discussed earlier. For the conditions when the regeneration is limited by the H_2 feed rate, NH_3 further reacts to form N_2 at the Pt/Ba interface and hence is not observed in the effluent. This is typically observed for the high dispersion catalysts at high temperatures. The above justification is given at the crystallite scale. This is also valid at the reactor scale, where NH_3 is likely to react with the stored NO_x downstream of the H_2 front under H_2 feed rate limited conditions.

The experimental data indicate that the peak N_2 concentration at the highest temperature (370°C) is less than the stoichiometrically expected value of 300 ppm (= Inlet H_2 concentration/5) for the 8% and 50% dispersion catalysts [1]. The expected value of the N_2 concentration is based on the following overall reaction during the regeneration [2]: $5H_2 + Ba(NO_3)_2 \rightarrow 5H_2O + BaO + N_2$. For the 8% dispersion catalyst, the peak N_2 concentration is 280 ppm, whereas it is 250 ppm for the 50% dispersion catalyst. This can be explained by the consumption of H_2 by the chemisorbed oxygen on Pt, due to which the effective H_2 concentration for reaction with the stored NO_x is less than the inlet concentration (=1500 ppm). The amount of chemisorbed oxygen on Pt at the start of regeneration increases with an increase in the Pt dispersion because of the increase in the amount of exposed Pt available for O_2 adsorption. Hence, the effective H_2 concentration for the reaction with stored NO_x decreases with an increase in dispersion, resulting in the decrease of peak N_2 concentration. Even though not shown here, the model is able to predict the decrease in peak N_2 concentration with an increase in the Pt dispersion, thus validating our hypothesis.

The model proposed in the current work can be used to explain some of the results reported in the literature. Castoldi et al. [44] reported an increase in the amount of NH_3 formed with an increase in the Ba loading of the catalyst. Also, a slow H_2 breakthrough was observed during the catalyst regeneration for high Ba loadings. However, an explanation of the finding was not given. Castoldi et al. [44] carried out the reduction at 350 °C, which is close to some of the experimental results of Clayton et al. [1] at 370 °C. Our model predictions and the experimental findings suggest that at high temperatures/NO_x diffusivities, the net amount of NH_3 formed increases with a decrease in the Pt dispersion. Hence, the experimental findings by Castoldi et al. [44] could be explained by a decrease of Pt dispersion with an increase in the Ba loading, which would result in an increase of NH_3 formation. Indeed, the decrease of Pt dispersion with an increase in the Ba loading was reported by Castoldi et al. [44]. This was ascribed to the fast and exothermic decomposition of Barium acetate precursor, leading to sintering of the Pt crystallites, and/or to the masking of the Pt crystallites by the Ba component.

It is instructive to analyze the effect of Pt dispersion on the regeneration of the LNT at a fixed temperature. Assume that the radius of the crystallite is inversely proportional to the Pt dispersion, i.e. $R_c = K/d$, where K is a proportionality constant [1]. Using this dependence of R_c on d in Eq. (7), we get:

$$S_E = \frac{N_{av} D_{Pt}^3 \pi M_{Pt_T} d}{2 A_{PF} K} \tag{44}$$

A similar analysis for the interfacial perimeter using Eq. (8) gives:

$$I_P = \frac{N_{av} D_{Pt}^3 \pi M_{Pt_T} d^2}{2 A_{PF} K^2} \tag{45}$$

As expected, Eq. (44) suggests that the surface area of exposed Pt varies linearly with the Pt dispersion (d). Eq. (45) shows that the total interfacial perimeter is proportional to the square of the Pt dispersion (d^2). Thus, a process which depends on the interfacial perimeter shows a stronger dependence on the Pt dispersion compared to a process which depends on the exposed surface area. It was justified earlier that the rate of NO_x reduction is proportional to the Pt/Ba interfacial perimeter. Reiterating, Eq. (45) suggests that the regeneration rate of the NO_x trap is proportional to the square of the dispersion. In contrast, the adsorption/desorption of reactants and products is proportional to the exposed surface area and hence linearly proportional to the dispersion. Even though catalysts having a fixed Pt loading have been studied in the current work, the analysis presented in this work can be used to study the dependence of catalyst loading on the H_2 and NH_3 breakthrough profiles, and the selectivity to NH_3. Eq. (44) shows that the exposed Pt surface area is proportional to the product of the Pt loading and the dispersion. Hence, if the dispersion can be increased by a finite factor, the catalyst loading can be reduced by the same factor in order to get the same exposed Pt area, thus reducing the catalyst costs. This calculation has even more value for the Pt/Ba interfacial perimeter, which depends on the product of the total Pt loading and the square of the catalyst dispersion (Eq. (45)). In effect, a small increase in the dispersion could result in a significant reduction in the total Pt loading, in order to obtain the same Pt/Ba interfacial perimeter.

In conventional LNT systems, NH_3 is an undesirable by-product. To the contrary, NH_3 generated using an LNT is beneficial for a system in which the LNT effluent is fed to a downstream SCR. It is observed from the experimental findings [1] and corroborated by the simulations that neither a high dispersion catalyst nor a low dispersion catalyst should be used separately over a range of temperatures in order to maximize (or minimize) NH_3 during the regeneration. Here, we propose a design to maximize the amount of NH_3 in the exhaust of a LNT over a range of temperatures. This would shift more of the NO_x reduction burden to the zeolite-based SCR catalyst, which is cheaper than the noble metals-based LNT catalyst. We consider two catalysts having different Pt dispersions sequentially positioned in the LNT, with the low dispersion catalyst in front of the high dispersion catalyst. At low temperatures, the low dispersion catalyst would not be active for storage or regeneration. The storage would primarily occur on the high dispersion catalyst. During the regeneration, the reductant would not be consumed while flowing through the low dispersion catalyst, because of low levels of NO_x stored and the low efficiency for NO_x reduction. However, the high dispersion catalyst would be active even at low temperatures. Hence, the reduction of NO_x would mainly occur on the high dispersion catalyst with a high selectivity to NH_3 because of the low temperatures (Fig. 10(c)). However, the Pt dispersion should not be too high, otherwise it could result in a high activity for reduction of NO_x by NH_3. In contrast, at high temperatures, the low dispersion catalyst would be active for the storage as well as regeneration. Hence, the storage would take place on the low dispersion catalyst and negligible amounts of NO_x would be stored on the high dispersion catalyst. During the regeneration, the reduction of NO_x would occur on the low dispersion catalyst, with a high selectivity to NH_3 because of the high temperatures (Fig. 10(a)). However, if NO_x is also stored downstream on the high dispersion catalyst, the NH_3 produced over the low dispersion catalyst would have a strong tendency to get reduced to N_2. Hence, the low dispersion catalyst needs to be designed in a way that it is sufficiently active at high temperatures to avoid NO_x release during the storage, which could adsorb on the high dispersion catalyst. Based on the earlier discussion related to the dependence of interfacial perimeter on the Pt loading and dispersion, the low dispersion catalyst in the design proposed above can be replaced by a high dispersion catalyst having a lower Pt loading. However, high dispersion catalysts might get deactivated due to the high temperatures encountered in a vehicle exhaust. Hence, catalyst aging in addition to the material costs needs to be considered in the design of these catalysts.

Experimental data on the effect of temperature during NO_x reduction is explained in this work by proposing the diffusion of stored NO_x as the rate determining process. Also, the work by Kumar et al. [37] and Sakamoto et al. [38] showed the existence of NO_x gradients in the BaO phase. However, there is lack of direct experimental evidence which rules out the possibility of the diffusion of H_2 in the BaO phase.

4. Conclusions

A model based on global kinetics is developed using detailed crystallite-scale catalyst features to investigate the effect of Pt dispersion and temperature during the regeneration of a lean NO_x trap. Experimental data for three catalysts having the same Pt loading but different dispersions is analyzed and simulations are performed to predict the experimental trends. It has been shown that the effect of dispersion can be explained by the varying average distance between the NO_x stored and the Pt/Ba interface and its effect on the stored NO_x transport process. The total interfacial perimeter between the Pt and Ba increases with an increase in the Pt dispersion, resulting in higher rates of reverse-spillover of NO_x. In addition, as the exposed Pt surface area increases, the consumption of H_2 by chemisorbed oxygen also increases.

The effect of temperature has been modeled by using temperature-dependent diffusivity of stored NO_x in the Ba phase. The model predicts that gradients in the stored NO_x concentration exist in the Ba phase. An analysis of the various characteristic times shows that the diffusion of stored NO_x in the Ba phase towards the Pt/Ba interface is likely the rate determining process. The analysis also shows that the selectivity towards NH_3 formation is governed by the relative rate constants of NH_3 formation and consumption, even though the absolute rates of both the reactions are high, i.e. the characteristic reaction times for NH_3 formation and consumption are lower than the characteristic diffusion times of stored NO_x. In line with the experiments, the model predicts that maximum NH_3 is produced for the 3.2% dispersion catalyst at high temperatures, for the 8% dispersion catalyst at intermediate temperatures, and for the 50% dispersion catalyst at low temperatures. This shift in the NH_3 concentration trends with temperature and Pt dispersion is explained by the change in the rate limiting process for the different catalysts for the range of temperatures studied. The model is also able to capture the decrease of peak N_2 concentration with an increase in the Pt dispersion, which has been explained by the consumption of H_2 by the chemisorbed oxygen on Pt.

The kinetics of NH_3 formation and consumption are assumed to be fast in the present work, which might not be valid at low temperatures. Clayton et al. [34] showed that H_2 was a better reductant than NH_3 at lower temperatures. Future modeling work should include the kinetic limitations due to NH_3, especially at lower temperatures ($<200\,^{\circ}C$). The model should also include the effect of diffusional limitations in the washcoat, either by solving the diffusion-reaction system in the washcoat or using the concept of internal mass transfer coefficients [56,57]. Finally, the concept of the exposed Pt surface area and the interfacial perimeter presented in this work could also be applied to TWC catalysts containing ceria, e.g. Yao and Yu Yao [58] reported an increase in the oxygen storage capacity with an increase in the metal loading, and it was ascribed to the synergistic reduction of ceria in close contact with the metal. Similar results were reported by Bedrane et al. [51,59]. Thus, the concept presented in this work could be used to study other catalytic systems, including TWCs and SCRs.

Based on the insights gained in this work, a method to maximize the total amount of NH_3 in the effluent of an LNT is proposed. The design involves placing two LNT catalysts having different dispersions in series, with the low dispersion catalyst in the front. At low temperatures, NH_3 would be produced primarily by the high dispersion catalyst, whereas, the low dispersion catalyst would be the main contributor to NH_3 formation at high temperatures. It is shown that analyzing the dependence of the Pt/Ba interfacial perimeter and the exposed Pt surface area on the catalyst dispersion and loading can be a useful tool in minimizing the catalyst loading and the associated costs.

Disclaimer

or reflect those of the United States Government or any agency thereof.

Acknowledgement

The work reported was supported by DOE-NETL (DE-FC26-05NT42630).

References

[1] R.D. Clayton, M.P. Harold, V. Balakotaiah, C.Z. Wan, Appl. Catal. B 90 (2009) 662.
[2] D. Bhatia, R.D. Clayton, M.P. Harold, V. Balakotaiah, Catal. Today 147 (1) (2009) S250.
[3] M. Sharma, M.P. Harold, V. Balakotaiah, Ind. Eng. Chem. Res. 44 (2005) 6264.
[4] M. Sharma, M.P. Harold, V. Balakotaiah, SAE J. 2005-01-3882 (2005).
[5] J. Xu, M.P. Harold, V. Balakotaiah, Appl. Catal. B 89 (1–2) (2009) 73.
[6] L. Olsson, H. Persson, E. Fridell, M. Skoglundh, B. Andersson, J. Phys. Chem. B 105 (2001) 6895.
[7] L. Olsson, R.J. Blint, E. Fridell, Ind. Eng. Chem. Res. 44 (9) (2005) 3021.
[8] B.R. Kromer, L. Cao, L. Cumaranatunge, S.S. Mulla, J.L. Ratts, A. Yezerets, N.W. Currier, F.H. Ribeiro, W.N. Delgass, J.M. Caruthers, Catal. Today 136 (2008) 93.
[9] A. Scotti, I. Nova, E. Tronconi, L. Castoldi, L. Lietti, P. Forzatti, Ind. Eng. Chem. Res. 43 (2004) 4522.
[10] P. Koci, M. Schejbal, J. Trdlicka, T. Gregor, M. Kubicek, M. Marek, Catal. Today 119 (2007) 64.
[11] P. Koci, F. Plat, J. Stepanek, M. Kubicek, M. Marek, Catal. Today 137 (2–4) (2008) 253.
[12] P. Koci, F. Plat, J. Stepanek, S. Bartova, M. Marek, M. Kubicek, V. Schmeißer, D. Chatterjee, M. Weibel, Catal. Today 147 (1) (2009) S257.
[13] C. Depcik, D. Assanis, K. Bevan, Int. J. Eng. Res. 9 (1) (2008) 57.
[14] A. Guthenke, D. Chatterjee, M. Weibel, N. Waldbußer, P. Koci, M. Marek, M. Kubicek, Chem. Eng. Sci. 62 (2007) 5357.
[15] Y. He, SAE J. 2006-01-0686 (2006).
[16] Y. Kim, J. Sun, I. Kolmanovsky, J. Koncsol, SAE J. 2003-01-1164 (2003) 61.
[17] G.C. Koltsakis, N.K. Margaritis, O.A. Haralampous, Z.C. Samaras, SAE J. 2006-01-0471 (2006).
[18] G. Konstantas, T. Stamatelos, Chem. Prod. Process Model. 2 (3) (2007), n.15.
[19] N.K. Margaritis, O.A. Haralampous, G.C. Koltsakis, Top. Catal. 42–43 (2007) 65.
[20] L. Olsson, D. Monroe, R.J. Blint, Ind. Eng. Chem. Res. 45 (26) (2006) 8883.
[21] C.M.L. Scholz, V.R. Gangwal, M.H.J.M. de Croon, J.C. Schouten, J. Catal. 245 (2007) 215.
[22] C.M.L. Scholz, K.M. Nauta, M.H.J.M. de Croon, J.C. Schouten, Chem. Eng. Sci. 63 (2008) 2843.
[23] R.S. Larson, J.A. Pihl, V.K. Chakravarthy, T.J. Toops, C.S. Daw, Catal. Today 136 (2008) 104.
[24] A. Lindholm, N.W. Currier, J. Li, A. Yezerets, L. Olsson, J. Catal. 258 (2008) 273.
[25] U. Tuttlies, V. Schmeisser, G. Eigenberger, Chem. Eng. Sci. 59 (22/23) (2004) 4731.
[26] A. Guthenke, D. Chatterjee, M. Weibel, B. Krutzsch, P. Koci, M. Marek, I. Nova, E. Tronconi, G.B. Marin, in: Advances In Chemical Engineering, vol. 33, AP, 2008, p. 103.
[27] S. Roy, A. Baiker, Chem. Rev. (2009), doi:10.1021/cr800496f.
[28] D. Bhatia, R.W. McCabe, M.P. Harold, V. Balakotaiah, J. Catal. 266 (1) (2009) 106.
[29] W.S. Epling, J.E. Parks, G.C. Campbell, A. Yezerets, N.W. Currier, L.E. Campbell, Catal. Today 96 (2004) 21.
[30] K.S. Kabin, P. Khanna, R.L. Muncrief, V. Medhekar, M.P. Harold, Catal. Today 114 (2006) 72.
[31] J.A. Pihl, J.E. Parks II, C.S. Daw, T.W. Root, SAE Tech. 2006-01-3441 (2006).
[32] L. Cumaranatunge, S.S. Mulla, A. Yezerets, N.W. Currier, W.N. Delgass, F.H. Ribeiro, J. Catal. 246 (1) (2007) 29.
[33] S.S. Mulla, S.S. Chaugule, A. Yezerets, N.W. Currier, W.N. Delgass, F.H. Ribeiro, Catal. Today 136 (2008) 136.
[34] R.D. Clayton, M.P. Harold, V. Balakotaiah, Appl. Catal. B 84 (2008) 616.
[35] L. Lietti, I. Nova, P. Forzatti, J. Catal. 257 (2008) 270.
[36] G. Zhou, T. Luo, R.J. Gorte, Appl. Catal. B 64 (2006) 88.
[37] A. Kumar, M.P. Harold, V. Balakotaiah, J. Catal 270 (2010) 214.
[38] Y. Sakamoto, K. Okumura, Y. Kizaki, S. Matsunaga, N. Takahashi, H. Shinjoh, J. Catal. 238 (2006) 361.
[39] A. Lindholm, N.W. Currier, J. Dawody, A. Hidayat, J. Li, A. Yezerets, L. Olsson, Appl. Catal. B 88 (2009) 240.
[40] U. Elizundia, R. Lopez-Fonseca, I. Landa, M.A. Gutierrez-Ortiz, J.R. Gonzalez-Velasco, Top. Catal. 42–43 (2007) 37.
[41] I. Nova, I. Castoldi, L. Lietti, E. Tronconi, P. Forzatii, F. Prinetto, G. Ghiotti, J. Catal. 222 (2004) 377.
[42] N.W. Cant, I.O.Y. Liu, M.J. Patterson, J. Catal. 243 (2006) 309.
[43] J.P. Schaffer, The Science and Design of Engineering Materials, Longman Higher Education, Chicago, 1994.
[44] L. Castoldi, I. Nova, L. Lietti, P. Forzatti, Catal. Today 96 (2004) 43.
[45] P.T. Fanson, M.R. Horton, W.N. Delgass, J. Lauterbach, Appl. Catal. B 46 (2003) 393.
[46] J. Dawodi, M. Skoglundh, S. Wall, E. Fridell, J. Mol. Catal. A: Chem. 225 (2005) 259.
[47] R.D. Clayton, M.P. Harold, V. Balakotaiah, AIChE J. 55 (3) (2009) 687.
[48] S.Y. Christou, A.M. Efstathiou, Top. Catal. 42/43 (2007) 351.
[49] M. Bowker, P. Stone, R. Smith, E. Fourre, M. Ishii, N.H. de Leeuw, Surf. Sci. 600 (2006) 1973.
[50] K. Ramanathan, V. Balakotaiah, D.H. West, Chem. Eng. Sci. 58 (2003) 1381.
[51] S. Bedrane, C. Descorme, D. Duprez, Catal. Today 75 (2002) 401.
[52] R. Lewis, R. Gomer, Nuovo Cimento 5 (1967) 506.
[53] D.A. Mullins, B. Roop, J.M. White, Chem. Phys. Lett. 129 (5) (1986) 511.
[54] M. Tringides, R. Gomer, J. Chem. Phys. 84 (1986) 4049.
[55] M. Tringides, R. Gomer, Surf. Sci. 155 (1985) 254.
[56] S.Y. Joshi, M.P. Harold, V. Balakotaiah, Chem. Eng. Sci. 64 (23) (2009) 4976.
[57] S.Y. Joshi, M.P. Harold, V. Balakotaiah, AIChE J. 55 (7) (2009) 1771.
[58] H.C. Yao, Y.F. Yu Yao, J. Catal. 86 (2) (1984) 254.
[59] S. Bedrane, C. Descorme, D. Duprez, Catal. Today 73 (2002) 233.